Received: 27 April 2023 | Revised: 22 June 2023 | Accepted: 30 June 2023

DOI: 10.1002/esp.5664

RESEARCH ARTICLE

ESPL WILEY

The evolution and preservation potential of englacial eskers: An example from Breiðamerkurjökull, SE Iceland

Amy Lally[1] | Alastair Ruffell[1] | Andrew M. W. Newton[1] | Brice R. Rea[2] | Thorsten Kahlert[1] | Robert D. Storrar[3] | Matteo Spagnolo[2] | Conor Graham[1] | Millie Coleman[1]

[1]School of Natural and Built Environment, Queen's University Belfast, Belfast, UK

[2]School of Geosciences, University of Aberdeen, Aberdeen, UK

[3]Department of the Natural and Built Environment, Sheffield Hallam University, Sheffield, UK

Correspondence
Amy Lally, School of Natural and Built Environment, Queen's University Belfast, University Road, Belfast BT7 1NN, UK.
Email: alally01@qub.ac.uk

Funding information
UKRI QUADRAT Doctoral Training Programme (DTP) studentship, Grant/Award Number: NE/S007377/1; Soulby Research Fund (QUB); British Society for Geomorphology; Quaternary Research Association

Abstract

Directly observing glacial drainage systems (englacial and subglacial) is challenging. The distribution, morphology and internal structure of eskers can provide valuable information about the glacial drainage system and meltwater processes. This work presents the annual evolution (meltout) and internal structure of an esker emerging from the Breiðamerkurjökull ice margin, southeast Iceland. Changes in esker morphology have been repeatedly mapped over a 1-year period using high temporal and spatial resolution data acquired by an uncrewed aerial vehicle (UAV). The internal architecture of the esker was investigated using ground-penetrating radar (GPR) surveys. These data are used to identify the dominant processes driving the formation of this englacial esker and to evaluate the preservation potential. The englacial esker was up to 2.6 m thick and ice-cored. A large moulin upglacier of the esker, which evolved into an englacial conduit, supplied meltwater to the englacial channel. Upglacier dipping debris-filled basal hydrofractures, formed by pressurised subglacial meltwater rising up the retrograde bed slope, likely supplied sediment to the englacial conduit. Over the 1-year period of observation the crest morphology evolved from flat- to sharp-crested and the esker footprint increased by a factor of 5.7 in response to post-depositional processes. The findings presented here indicate that englacial eskers may have low preservation potential due to post-depositional reworking such as slumping through ice-core meltout and erosion by later meltwater flow. As englacial eskers may not be preserved in the landscape, they could represent important glacial drainage system components that are not currently captured in palaeo-ice sheet reconstructions. This work highlights the value of creating a time series of high-temporal resolution data to quantify morphological evolution and improve glacial process-form models.

KEYWORDS
englacial glacial drainage system, esker, glacial geomorphology, glacial process-form regimes, GPR, Iceland, landform evolution, temperate glacier, UAV

1 | INTRODUCTION

Repeated surveying and analysis of modern glacial landscapes is crucial for refining glacial process-form models and enhancing our understanding of the spatiotemporal evolution of glacial geomorphology (Guðmundsson & Evans, 2022). Studying glacial landforms in contemporary settings can establish modern process-based analogues that enhance our understanding of palaeo-glaciated landscapes

(Evans, 2003; Benn & Evans, 2010 and references therein). The development of process-form regimes in modern glacial environments establishes links between the processes that drive landform development and associated glaciological conditions, such as topographic setting, surge activity and thermal regime (Bennett & Evans, 2012; Chandler et al., 2020; Ely et al., 2017; Evans, 2011; Evans et al., 2022; Evans & Orton, 2015; Price, 1969; Rea & Evans, 2011; Spedding & Evans, 2002; Tomczyk et al., 2019). Modern process-form analogues have been applied to comparable landform assemblages in ancient glaciated terrain, allowing for the reconstruction of palaeoglaciological conditions (e.g. Evans et al., 2020; Sutherland et al., 2019).

Investigating the spatial and temporal evolution of meltwater-generated landforms provides valuable insights into meltwater pathways/networks as direct observations are often hindered by logistical and safety challenges. To date, most observations of glacial drainage systems have been made indirectly through geophysical methods [e.g. ground-penetrating radar (GPR)] and dye-tracing experiments (Burke et al., 2008; Church et al., 2020; Cowton et al., 2013; Gulley et al., 2014; Nienow et al., 1998) with rare direct observations obtained using glacio-speleology (Benn et al., 2009; Gulley & Benn, 2007; Temminghoff et al., 2019). Mapping the distribution of meltwater-generated landforms, revealed following ice-margin retreat, can be also used to reconstruct snapshots of subglacial drainage systems (Aylsworth & Shilts, 1989; Clark & Walder, 1994; Storrar et al., 2020) during deglaciation.

Eskers, which record the location of channelised drainage, are sinuous ridges of glaciofluvial sediment deposited in an ice-walled channel (Brennand, 2000; Huddart et al., 1999; Price, 1969). Eskers are abundant across the beds of palaeo-ice sheets and have been identified in contemporary glacierised environments (Bennett & Evans, 2012; Burke et al., 2008; Evans et al., 2023; Evans & Twigg, 2002; Howarth, 1971; Huddart et al., 1999; Knudsen, 1995; Price, 1969; Storrar et al., 2015). Eskers deposited englacially have also been observed in ancient and modern glacial settings (Bennett & Evans, 2012; Burke et al., 2008; Evans et al., 2023; Howarth, 1971; Perkins et al., 2016; Price, 1969). Englacial eskers serve as records of englacial hydrology, which plays a crucial role in delivering supraglacial meltwater to the subglacial environment where it can influence ice dynamics (Catania et al., 2008; Das et al., 2008; Joughin et al., 2008; Zwally et al., 2002). Along with Shreve-type englacial conduit model of formation, other mechanisms include exploitation of fractures (Fountain et al., 2005; Stenborg, 1969), permeable debris-filled structures (Gulley & Benn, 2007), hydrofracturing (Boon & Sharp, 2003; Rothlisberger & Lang, 1987) and incision of supraglacial streams which then close over by the cut and closure mechanism (Fountain & Walder, 1998; Gulley et al., 2009).

GPR can image subglacial and englacial drainage systems by penetrating through ice (Church et al., 2020; Church et al., 2021; Gusmeroli et al., 2008; Hansen et al., 2020; Karušs et al., 2022; Matsouka et al., 2007; Murray et al., 2008; Phillips et al., 2013) and provides a valuable tool to investigate the internal architecture of glacial landforms. This geophysical method is particularly useful in areas where sediment exposures are lacking (e.g. Harrison et al., 2022; Pellicer & Gibson, 2011; Spagnolo et al., 2014) and has been used to investigate eskers in both modern and ancient glacial settings (Burke et al., 2008; Perkins et al., 2013, 2016; Stoker et al., 2021).

In this paper, geomorphological mapping, high-spatial resolution aerial imagery and GPR are combined to document the emergence and evolution of an englacial esker from Breiðamerkurjökull, southeast Iceland (Figure 1). The system was surveyed three times over the space of a year. This unprecedented temporal and spatial resolution allows an evaluation of the key controls on the formation processes and preservation potential of eskers, with implications for their use to decipher palaeo-glacial drainage systems.

2 | BREIÐAMERKURJÖKULL SETTING AND PREVIOUS ESKER RESEARCH

Breiðamerkurjökull is a piedmont lobe outlet glacier located in southeast Iceland and is the fourth largest glacier draining from the Vatnajökull ice cap (Guðmundsson et al., 2017) (Figure 1a). It consists of three main flow units: the western, central and eastern units (Guðmundsson & Evans, 2022). In the last 120 years, Breiðamerkurjökull has retreated over 7 km, at between 70 and 200 ma^{-1} (Guðmundsson et al., 2019), exposing more than 115 km^2 of the former subglacial bed (Guðmundsson et al., 2017).

The proglacial area of Breiðamerkurjökull is characterised by up to 1.3 m of till, underlain by up to 50 m of unconsolidated glaciofluvial sediments draped over fractured igneous bedrock (Boulton et al., 2007a). The low-lying unconfined topography facilitates the formation of extensive glacial outwash plains (Guðmundsson & Evans, 2022). The western and eastern flow units terminate in proglacial lakes formed in overdeepened troughs, eroded during periods of more extensive ice cover (Evans & Twigg, 2002).

Mapping at Breiðamerkurjökull, which began in the early 1900s (e.g. Lister, 1951; Todtmann, 1960) provided a historical record of landforms to inform later mapping efforts; see Evans (2009) and Guðmundsson & Evans (2022) for a comprehensive review of geomorphological research at Breiðamerkurjökull. Repeat mapping from historical imagery has provided a unique time series of Breiðamerkurjökull proglacial landscape evolution spanning 1945, 1965, 1998 and 2018 (Evans & Twigg, 2000; Guðmundsson & Evans, 2022; Howarth & Welch, 1969a, 1969b). Furthermore, Breiðamerkurjökull has been the subject of numerous process-form studies (Price, 1969; Price & Howarth, 1970; Welch & Howarth, 1968) and was central to the development of the active temperate glacier landsystem model by Evans & Twigg (2002).

Eskers have been reported across the foreland of all three flow units (Evans & Twigg, 2002; Howarth, 1971; Price, 1969; Storrar et al., 2015, 2020). Complex esker systems have been documented emerging from stagnant ice (Price, 1969, 1982; Storrar et al., 2015), englacial eskers have been observed melting out of the ice margin (Howarth, 1971; Price, 1969), and subglacial eskers have been revealed as proglacial lakes drain (Guðmundsson & Evans, 2022).

This study focuses on an esker located at the ice margin of the central flow unit, Esjufjallajökull, which is the only predominantly land-terminating flow unit (Figure 1). The foreland west of the esker is dominated by kame and kettle topography, whereas the east is characterised by subglacially streamlined till deposited on a topographic high.

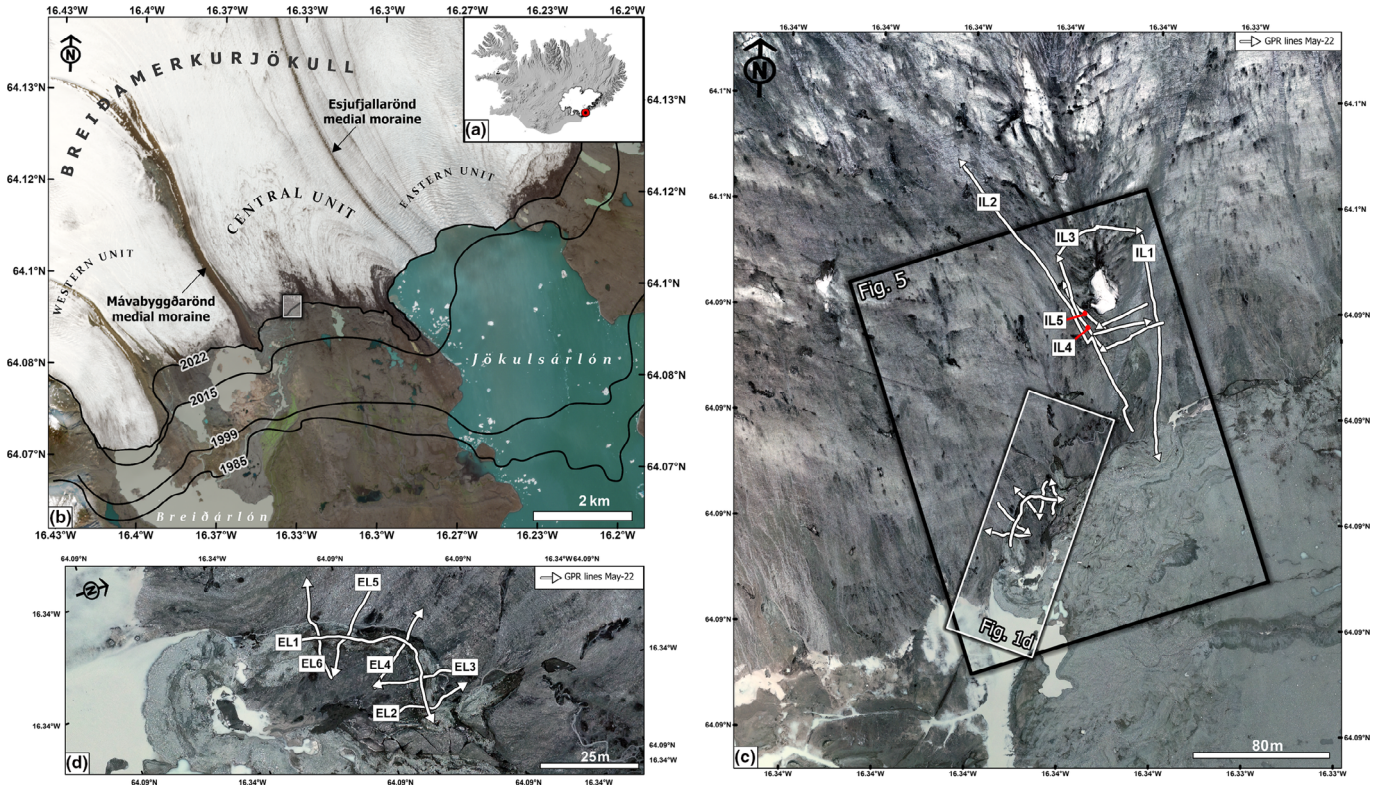

FIGURE 1 (a) Copernicus EU-DEM of Iceland and Vatnajökull ice cap with Breiðamerkurjökull marked by the red dot; (b) Breiðamerkurjökull and associated foreland (Sentinel-2 harmonised true colour image from 6 May 2022) with extent of Figure 1c (white box) shown. The central unit (Esjufjallajökull) is delineated by two medial moraines: Mávabyggðarönd to the west and Esjufjallarönd to the east. Several terminus locations are noted from 1985 to present; (c) GPR survey lines collected in May 2022, overlain on the May 2022 orthomosaic generated from UAV data. The arrows indicate the acquisition direction. On-ice GPR lines shown in Figure 8 are labelled IL1-5. Extents for Figures 1d and 3 are shown; (d) Zoomed-in view of esker cross and crestline (Figure 7, EL1-6) GPR profiles, overlain on the May 2022 orthomosaic. [Color figure can be viewed at wileyonlinelibrary.com]

3 | METHODS

3.1 | Uncrewed aerial vehicle data acquisition and field observations

To capture the landform emerging from the ice, the study area (Figure 1c) was surveyed using a DJI Phantom 4 RTK quadcopter UAV three times over a 1-year period: 5–10 September 2021, 6–12 May 2022 and 5–8 September 2022.

Images were processed and DEMs created in Agisoft Metashape v1.8.1, following a structure-from-motion photogrammetry with multi-view stereopsis workflow (Westoby et al., 2012). Although data were collected in RTK, which have a ~0.015 m position accuracy (Lamsters et al., 2022), additional ground control points were taken in May 2022. The September 2021 and 2022 DEMs were spatially corrected using the May 2022 DEM. The DEMs and orthomosaics have ~6 cm horizontal resolution. The three temporal DEMs were compared in ArcGIS Pro to quantify topographic change. Esker footprints were determined by break of slope, elevation changes and the change from ice to gravel. To prevent visual distortion while ensuring the data are readable by those with colour-vision deficiency (Crameri et al., 2020), the Scientific Colour Map Batlow (Crameri, 2020) was used for the visualisation of mapped outputs.

Repeat morphometric analyses from the DEMs included esker ridge length, footprint, sinuosity, continuity and prominence (Figure 2). Prominence of the esker (i.e. esker height above the surrounding glacier and foreland) was calculated by interpolating DEM pixel values from the surrounding ice, 1 m from the esker footprint vertices. The sinuosity was calculated as the ratio between the ridge length and the straight-line distance between the proximal and distal ends of the esker (Storrar et al., 2014). Continuity was calculated by the percentage of gaps along the full interpolated crestline length. The esker was photographed and described during each field campaign to identify sedimentological facies.

3.2 | GPR data acquisition and processing

The purpose of the geophysical surveys was to examine the small-scale sedimentary architecture of the esker and the drainage network of the surrounding glacier. GPR common offset data were collected in May 2022 using a Mala GroundExplorer (GX) 450- and 160-MHz shielded antennas (in-built parallel broadside configuration) connected to a Mala GX controller, using wheel mode via the odometer attached to a mounting block on each antenna and pulled on skid plates.

One crestline and five cross-profiles were collected across accessible areas of the esker using both frequencies (Figure 1d). Additional GPR profiles were collected upglacier between the esker and a large moulin to the north (Figure 1c) to aid in the identification of possible subglacial/englacial channels connected to the esker system.

Raw GPR data were processed using ReflexW v7.5.9 (Sandmeier, 2006). The processing sequence comprised static

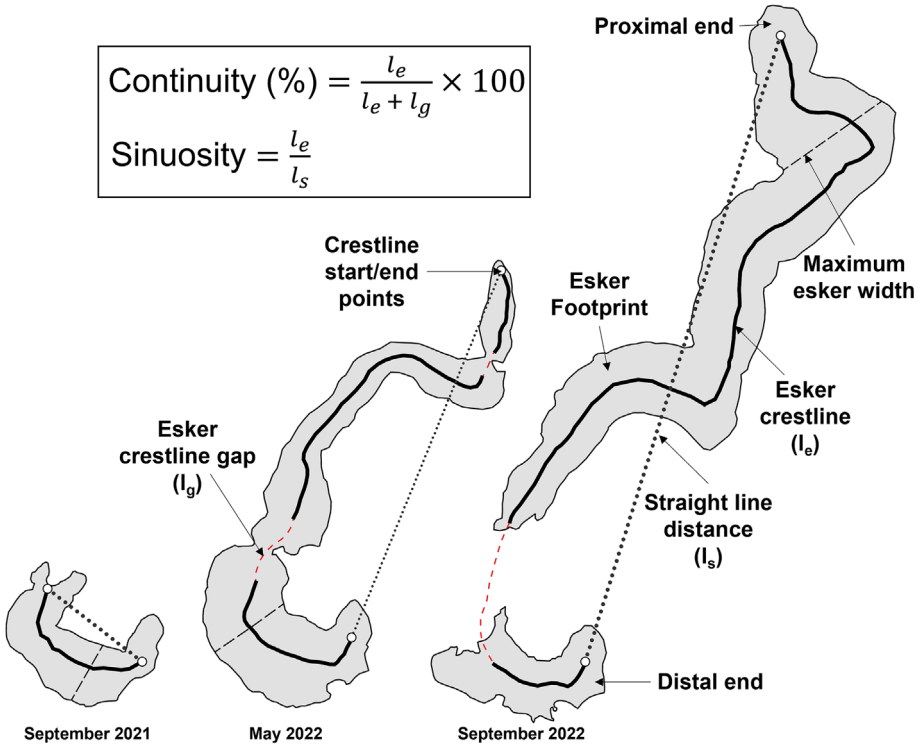

FIGURE 2 Esker outlines over the three study periods: September 2021, May 2022 and September 2022. Parameters used in the morphological analysis include esker crestline (le), esker footprint (grey infill), esker crestline gaps (lg), maximum width from esker base (black dashed line), start and end points of the esker crests (white circles) and the straight-line distance between them (black dotted line). [Color figure can be viewed at wileyonlinelibrary.com]

correction for time-zero drift, dewow high-pass filter, background removal and topographic correction (RTK-derived DEM). Developing a velocity model of the substrate was problematic due to subsurface heterogeneities (e.g. debris content variations, water inclusions, fractures, caves, range of sediment/clast sizes). Although depths are not considered accurate, due to stratigraphic and lateral changes in substrate composition and water content, and thus dielectric permittivity, for the purpose of comparing the GPR lines, a velocity of 0.152 mns^{-1} was used for glacier ice (Burke et al., 2008; Murray et al., 2000). For esker sediments, a velocity of 0.1 mns^{-1} was used for the crest profile in accordance with other GPR esker studies (e.g. Livingstone et al., 2017; Stoker et al., 2021).

Reflections and facies were determined based on reflection motif, amplitude, continuity, shape and degree of reflectivity/opacity (Annan, 2009; Beres & Haeni, 1991; Jakobsen & Overgaard, 2002; Van Overmeeren, 1998) and contextual information gathered during each field campaign. Processed profiles were displayed and interpreted using Inkscape, an open-source vector graphics software.

4 | RESULTS AND INTERPRETATION

4.1 | Morphological and sedimentological analysis

The time series of orthomosaics and DEMs is depicted in Figure 3 along with the summary of the morphological analysis in Table 1. The esker footprint area and maximum width increased ×5.7 and ×1.9, respectively, in 1 year.

Three main sedimentary facies were identified. Facies 1 consists of poorly sorted clast-supported gravels with no internal bedding. In September 2021, the esker exposures were composed entirely of Facies 1. By 2022, this facies was confined to the proximal and distal portions of the esker. Facies 2, which was up to 2 m thick, is characterised by poorly sorted matrix-supported gravels, deposited in aggrading gravel beds dipping downglacier (e.g. Figure 4f). The lower unit boundary of Facies 2 was not exposed due to slumped flank deposits. Facies 3 is well-sorted fine-grained deposits, up to 1 m thick, composed of tephra, sands and silts that usually overlie Facies 2. Facies 3 contains asymmetric current ripples, cross-lamination (e.g. Figure 4k) and is often interrupted by <0.3-m-thick gravel beds (e.g. Figure 4j), indicating variations in flow velocities during deposition. Slump deposits, up to 0.5 m thick lying over ice (Figure 4n), were noted along the flanks of the esker in all three study periods. These slump deposits contained varying amounts of fine material.

In September 2021, the exposed (distal end) esker was broad and flat-crested with steep flanks (up to 86°) (Figure 4a). By May 2022, the esker was sharp-crested along the distal end and flat-topped upglacier (Figure 4b). The broad flat-crested areas in May 2022 became sharp to round-crested by September 2022, as the underlying ice melted, and material slumped down the flanks. In September 2022, the distal part of the esker became round-crested with sparse flat-crested areas (Figure 4c). The increase in footprint and changes to slope angles occurred overtime due to reworking and slumping of crest and flank deposits.

A time series of elevation profiles across and along the esker are shown in Figure 5. Over the measurement year, ~8 m of ice overlying the proximal portion of the esker melted with the exposed distal section lowering (due to ice-core meltout) and being eroded. The exposed crestline in May 2022 remained mostly unchanged throughout the melt season, indicating that ice-core meltout was insignificant over the summer months (Figure 5b, Profile F).

The high sinuosity (1.17–1.56), areas of channel unroofing (Figure 4h) and the sharp-crest are indicative of deposition in an englacial channel near the ice surface as described by Perkins et al. (2016). The fine-grained broad-crested portions of the esker (e.g. Figure 4e) indicate deposition in an englacial tunnel during the

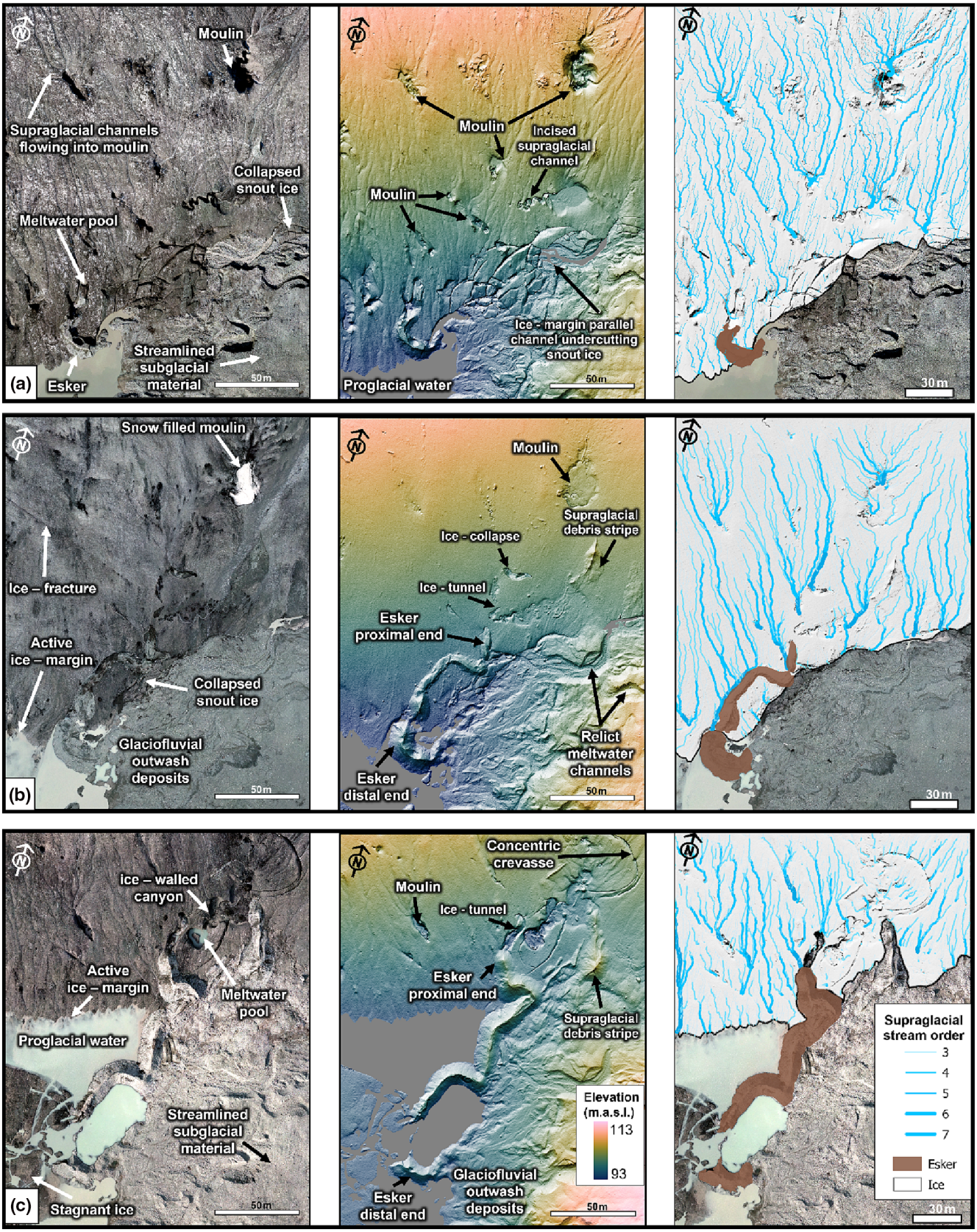

FIGURE 3 Orthomosaic, DEM and supraglacial hydrological analysis (flow direction and accumulation analysis) for (a) September 2021, (b) May 2022 and (c) September 2022. Proglacial water is masked in the DEM (grey shaded areas) [DEM error—2.06 cm (horizontal); 0.59 cm (vertical); 2.15 cm (total)]. [Color figure can be viewed at wileyonlinelibrary.com]

gradual shutdown of the channel over the winter period, consistent with the findings of Huddart et al. (1999) and Shreve (1985). As the esker crestline has been shown to evolve into a sharp- or round-crested form in response to post-depositional slumping, it is not comparable to flat-crested subglacially deposited forms preserved in the palaeoglaciological record (Perkins et al., 2016). The variation in

TABLE 1 Summary statistics and morphological analysis for the esker over the three field visits.

Morphometric	September 2021	May 2022	September 2022
Crest length (m)	38.5	110.9	150.2
Area (m^2)	408	1294	2340
Continuity (%)	100	84	75
Continuity (count)	1	3	3
Sinuosity	1.65	1.71	1.56
Maximum width (m)	12.4	16.5	23.5
Max prominence (m)	3.7	5.5	5.4
Average height (m.a.s.l.)	99.3	99.5	99.9
Max height (m.a.s.l.)	100.2	100.7	102.1
Min height (m.a.s.l.)	96.3	96.8	96.7
Average slope (°)	30.6	29.9	23.3
Max slope (°)	85.8	78.6	81.5
Min slope (°)	0	0	0
Proportion of the esker south of the active ice margin (%)	23	48.8	84

morphometric parameters over 1 year highlights the influence of post-depositional processes on the morphological evolution of ice-cored englacial eskers as the ice melts out.

4.2 | Supraglacial hydrological network analysis

The supraglacial drainage network (Figure 3), controlled by the ice surface slope, demonstrates that supraglacial meltwater was concentrated towards the large moulin and a series of smaller moulins north of the esker location. The large moulin likely fed the esker until the channel was abandoned in response to ice-margin thinning. From May to September 2022, the large moulin had evolved into an ice-walled/floored canyon with concentric crevasses draining supraglacial channels. The esker location was once in a zone of supraglacial meltwater capture; however, over the 2022 meltwater season, the area underwent topographic reversal, with meltwater now diverted around or under the esker system (e.g. Figure 4m).

4.3 | Radar facies identification and interpretation

The complexity of this area of the Breiðamerkurjökull ice-marginal environment is highlighted by the six facies identified in the radargrams (Figure 6).

4.3.1 | Radar Facies 1

Radar Facies 1 (RF1) represents undulating, sub-horizontal, continuous to moderately continuous reflections often associated with fault structures. RF1 is interpreted as the esker (Figure 7) and glaciofluvial deposits in the foreland (Figure 8, IL1).

RF1 occupies a depression in the ice in the cross-profiles, consistent with glaciofluvial deposition in an ice-walled channel and is up to ~2.5 m thick along the crest. It also indicates that thermal erosion of the channel base occurred prior to the initial deposition.

Faults associated with RF1 appear to dictate the location of the esker and thus channel geometry (Figure 7, EL2-2L6). These faults rarely disrupt primary bedding, indicating that the structures predate the glaciofluvial deposition, which suggests englacial conduits develop via exploitation of weaknesses in the ice (Bennett et al., 2000; Roberts et al., 2000). Smaller faults that disrupt bedding along the crest are interpreted as post-depositional normal faulting in response to the removal of supporting ice walls (Brennand, 2000; Fiore et al., 2002; Lovell et al., 2019; McDonald & Shilts, 1975).

4.3.2 | Radar Facies 2

Radar Facies 2 (RF2) represents areas of radar signal attenuation in both the 160 and 450 MHz GPR profiles. In cross-profile EL2-6 (Figure 7), RF2 underlies the trough/basin-shaped bottom reflection of RF1 and is associated with velocity pull-downs each side of the attenuated area.

An explanation for the attenuation is the presence of clay-sized sediments or saturated sands/silts being the initial material deposited in the englacial conduit. Grey-green cohesive clay mounds were observed melting out onto the ice surface, and light brown clays were found in the matrix of subglacial sediment exposures. Clay-sized sediments may cause radar wave attenuation due to a lack of polarity, while a clay mineral fraction in the sediments can significantly reduce the propagation depth of the radar waves obscuring deeper reflections due to the increased conductivity and dielectric constant.

The attenuation could also be an artefact of GPR movement across the steep flanks of the esker (Neal, 2004). However, the esker crestline and foreland profiles containing RF2 are not impacted by steep slopes, and thus, RF2 are interpreted as 'real' radar responses.

4.3.3 | Radar Facies 3 and 4

Radar Facies 3 (RF3) and 4 (RF4) represent the glacial ice. RF3 occurs near the surface with minimal internal reflections and is taken to

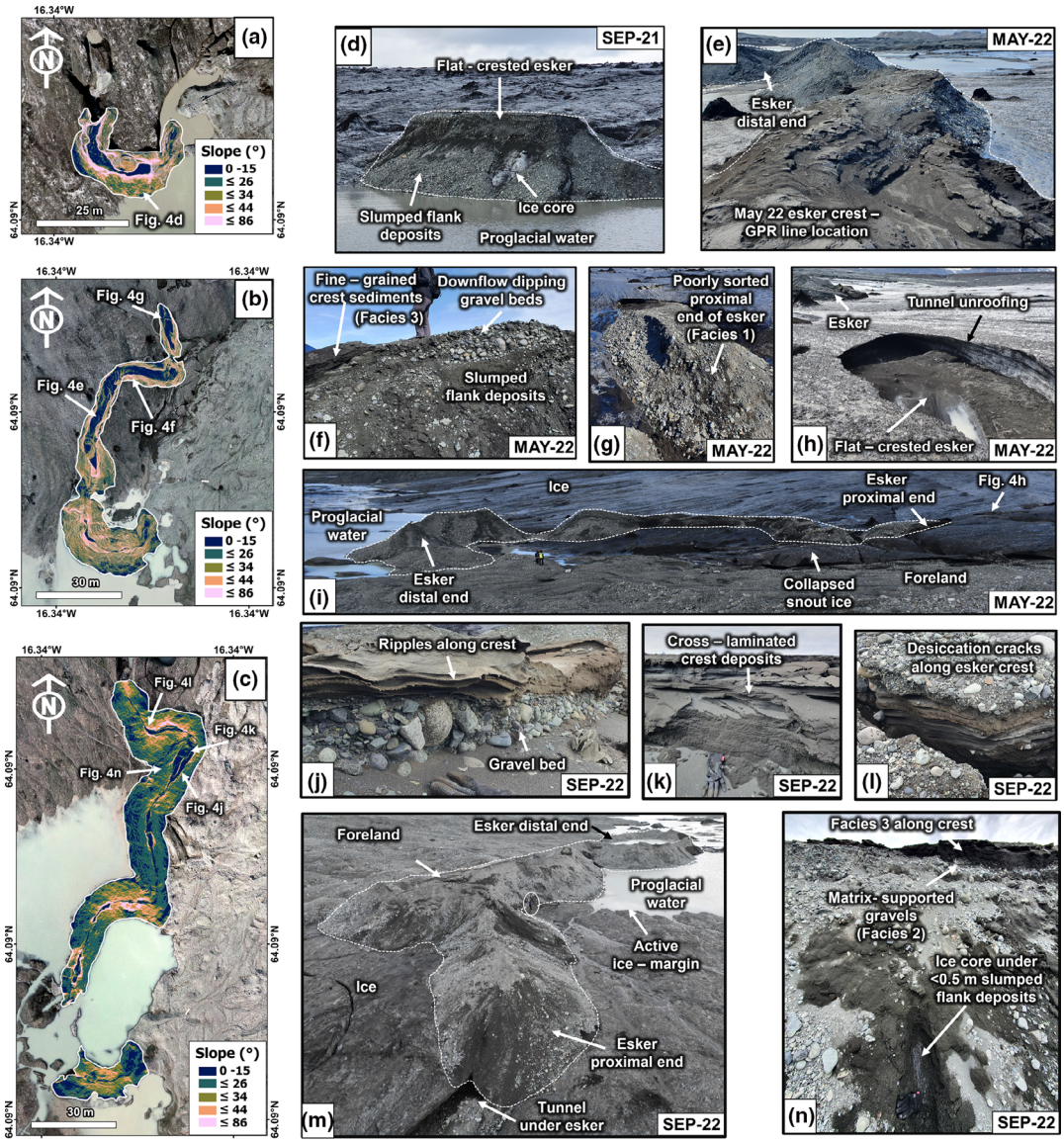

FIGURE 4 Slopes across the esker footprint for (a) September 2021, (b) May 2022 and (c) September 2022. Field photos for all three study periods: (d) September 2021 esker with a field photo facing northwest; note the flat crest, steep flanks and ice core; (e) the broad-crested esker area where the May 2022 GPR lines were taken, photo facing west; (f) headward accreted gravel beds dipping down glacier (photo facing northwest); (g) proximal end of the esker emerging from a tunnel, composed of poorly sorted gravels (Facies 1) (photo facing north); (h) 1 m upglacier from Figure 4g, unroofed tunnel revealing flat-topped crest deposits (photo facing south); (i) downglacier side of the esker, people for scale (1.8 m) (photo facing northwest); (j) differential sorting along the esker crest, rippled sandy sediments overlying gravel layer indicates variations in meltwater energy (photo facing north); (k) Facies 3 cross-laminated sands and silts along esker crest (photo facing south); (l) cracks and detached slabs of sediment were observed along the September 2022 esker crest likely due to desiccation of sand laminae; (m) UAV image of the esker facing southwest, circled person for scale (1.7 m); (n) steep esker flanks; the ice core was covered with gravity sorted slumping deposits (photo facing southeast). [Color figure can be viewed at wileyonlinelibrary.com]

represent 'clean ice'. Enhanced noise and internal reflections of RF4 are taken to indicate debris-rich ice. The transition between RF3 and RF4 is usually gradual and represents a transition from less to more debris-rich ice with depth. Ice nearer the margin was composed of RF4, with RF3 restricted to shallower areas upglacier.

4.3.4 | Radar Facies 5

Radar Facies 5 (RF5) is characterised by high-amplitude, discontinuous, planar bedding, which primarily dips up glacier, becoming sub-horizontal closer to the ice margin. These near-parallel, high-amplitude reflections do not undulate like the glaciofluvial deposits (RF1). RF5 is always normal polarity, indicating a lower velocity than the surrounding glacial ice. Due to signal attenuation (i.e. RF2) under the esker core, RF5 cannot be picked below the esker but is imaged either side of the cross-profiles (Figure 7), extending from the ice-bed interface up into the ice and extending from the ice surface down into the ice (Figure 8).

The areas where RF5 extends to the ice-bed interface are assumed to be genetically similar to the upglacier dipping sediment-filled fractures observed by Roberts et al. (2000) at Skeiðarárjökull. Here, sands and gravels were observed melting out on the surface of the snout (Figure 9b) and from the sides of the ice-walled canyon in September 2022, providing further evidence for the presence of englacial debris. Similar features were documented in Iceland

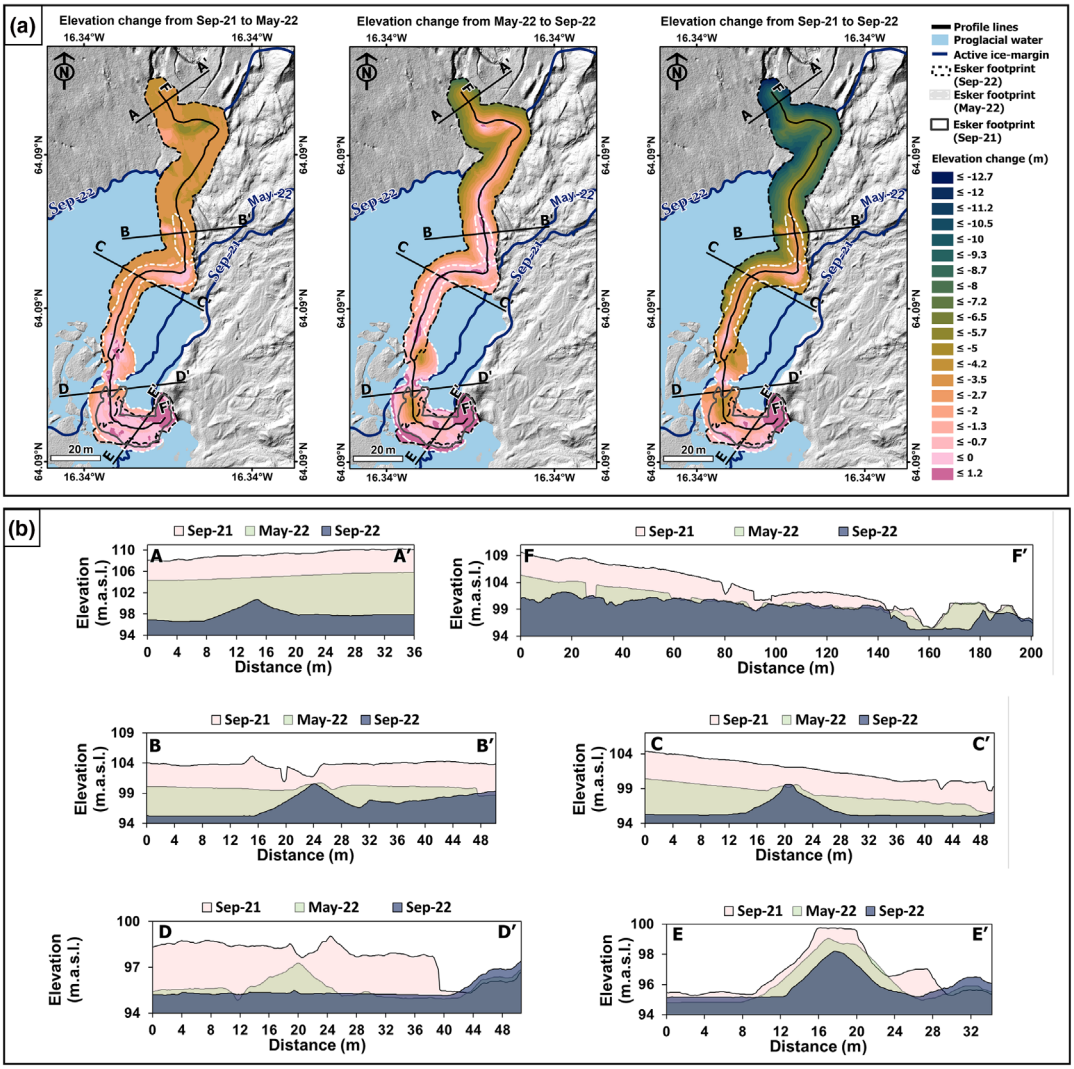

FIGURE 5 (a) Computed elevation differences along and across the esker crest between each study period. The elevation profile A–F locations, overlying the September 2022 Hillshade; (b) elevation profiles for a number of locations across the crest (A–E) and along the crest line (F) generated from each DEM. [Color figure can be viewed at wileyonlinelibrary.com]

(Bennett & Evans, 2012) and Svalbard (Evans et al., 2022; Ewertowski et al., 2019). RF5 is imaged up- and downglacier of the esker cross-sections (EL2-6) suggesting the entrained debris may have supplied the englacial conduit with sediment.

RF5 likely represents clastic dykes (water escape structures) formed by sediment entrainment into upward propagating hydrofractures (Roberts et al., 2000). Bottom-up hydrofracturing occurs when basal water pressures are approaching or exceed the pressure exerted by the overlying ice and can occur at lower water pressures in the presence of tensile stresses in the ice (Rea & Evans, 2011). Top-down hydrofractures can propagate too under high tensile stresses but only to significant depths when the fractures are water filled (Benn et al., 2009; Rea & Evans, 2011). Unless there is abundant supraglacial sediment, top-down hydrofractures are unlikely to contain sediment in the quantity required to form the englacial esker documented here.

Shallow-dipping reflections, extending from the ice surface down ~1–2 m, were visible on all lines and may represent tephra-filled folia, like those observed by Burke et al. (2009). The dip direction varies depending on deformation patterns, which were visible on the surface across the study area (e.g. Figure 9c).

4.3.5 | Radar Facies 6

Radar Facies 6 (RF6) comprises high-amplitude, discontinuous reflectors that occur deeper than RF5. Due to low dielectric contrast between unconsolidated subglacial sediments at the ice-bed interface and debris-rich ice, strong subglacial bed reflections are not often found in the GPR profiles. Similar to Church et al. (2020), locations where RF6 is imaged may represent saturated basal sediments or water-filled cavities, with a higher radar wave amplitude than unsaturated sediments. The phase of the deep reflectors RF6 remains consistently normal polarity (+ − +) indicating a velocity slow-down; therefore, RF6 does not represent subglacial air-filled voids. The subglacial bed reflection in IL2 (Figure 8) dips upglacier and is indicative of the glacier retreating over a retrograde bed.

4.3.6 | Diffractions

Zones of diffraction were noted ~1–1.5 m below the esker crestline; adjacent and deeper reflections are obscured by these diffractions. These may represent clusters of coarse cobble gravels, where the

Radar Facies	Radar signature 160 MHz	Radar signature 450 MHz	Field photos	Interpretation
RF1	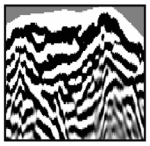	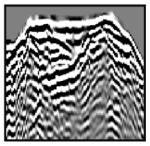		**Glaciofluvial deposits** - esker and outwash sediments
RF2	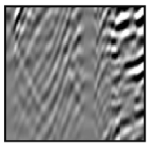			**Clay-rich deposits** - signal attenuation esker ridge and subglacial till
RF3	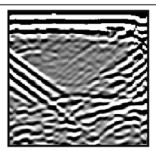	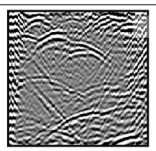		**Temperate glacial ice** - "clean ice" minimal internal reflections
RF4	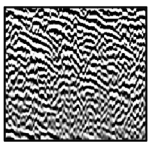		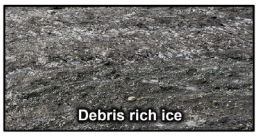	**Debris rich basal ice** - enhanced noise and abundant internal reflections
RF5		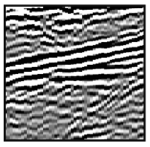	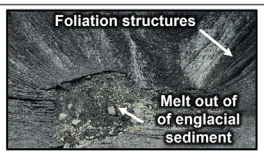	1. **Basal hydrofractures** - with entrained englacial debris 2. **Tephra-filled foliation** - if extended from the surface
RF6			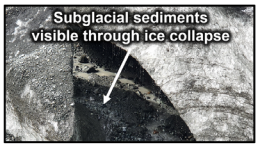	**Subglacial bed** - or areas of saturated subglacial sediments
Diffractions		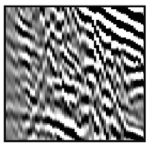	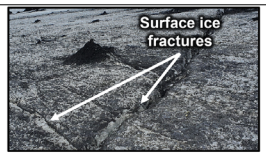	1. **Ice fractures** 2. **Diffractions from point sources** - clusters of gravel, cobbles or boulders
Hyperbolic reflections (+-+)				1. **Englacial channels** - or water inclusions 2. **Large point sources** - cobbles or boulders
Hyperbolic reflections (-+-)	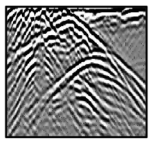	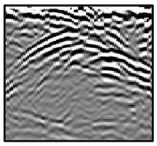		**Ice caves** - tunnels or voids below the surface
Ringing reflections	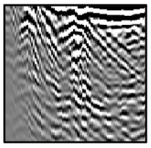	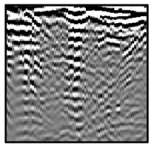		1. **Supraglacial channel** - pull-down of ground wave 2. **Englacial meltwater channels/pools** - originates below the surface

FIGURE 6 A description and interpretation of six radar facies and other features identified in the GPR profiles. [Color figure can be viewed at wileyonlinelibrary.com]

receiver is collecting reflections from individual clasts, similar to beach GPR profiles (Neal, 2004). Diffraction zones were also imaged in the on-ice lines at the surface and concentrated at the snout (e.g. Figure 8, IL1). These areas could indicate increased fracturing of the ice or increased debris concentration, resulting in a zone of enhanced noise.

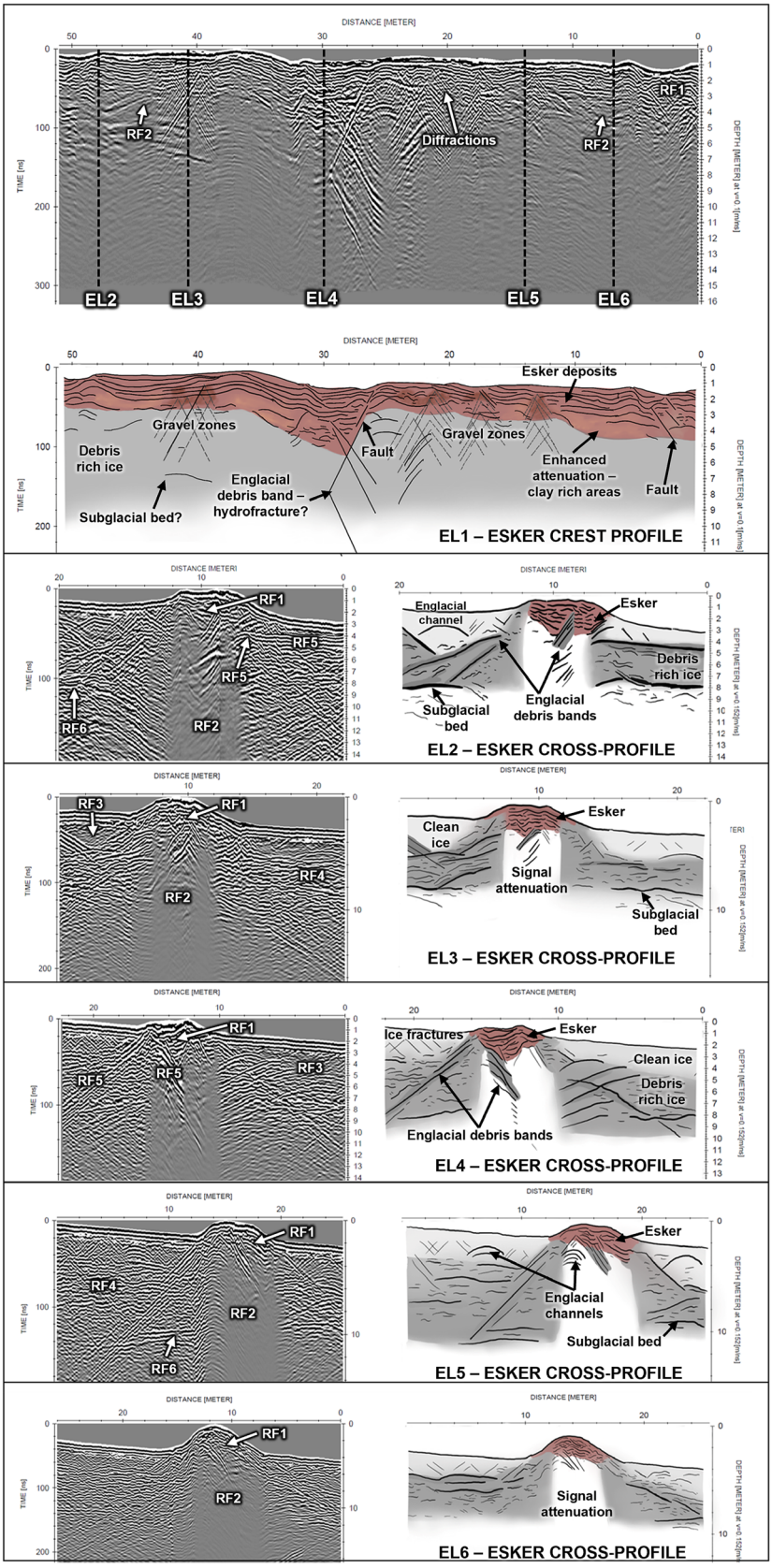

FIGURE 7 Topographically corrected 160-MHz GPR lines and the associated interpretation for the esker GPR lines (EL), the location of each line is presented in Figure 1d. Where each of the cross-profiles (EL2-6) intersects with the crestline (EL1) is labelled on the EL1 radargram. The esker sediments are shown in brown, with clean ice (light grey) and debris-rich ice (dark grey). [Color figure can be viewed at wileyonlinelibrary.com]

4.3.7 | Hyperbolic reflections and associated multiples

A normal polarity (+ − +) hyperbolic reflection (4 m depth) and associated multiples were imaged under RF1 in EL5 (Figure 7), indicating a velocity decrease in the radar wave compared to the overlying esker sediments and ice. This set of reflections is interpreted as an englacial meltwater channel located beneath the esker. This is supported by the observation, in September 2022, of a tunnel beneath the upglacier end of the esker (Figure 4m).

Normal polarity hyperbolae dominate both the clean ice (RF3) and the debris-rich ice (RF4), which may represent englacial channels or water inclusions. Ringing reflections associated with a pull-down of the ground wave represent supraglacial channels.

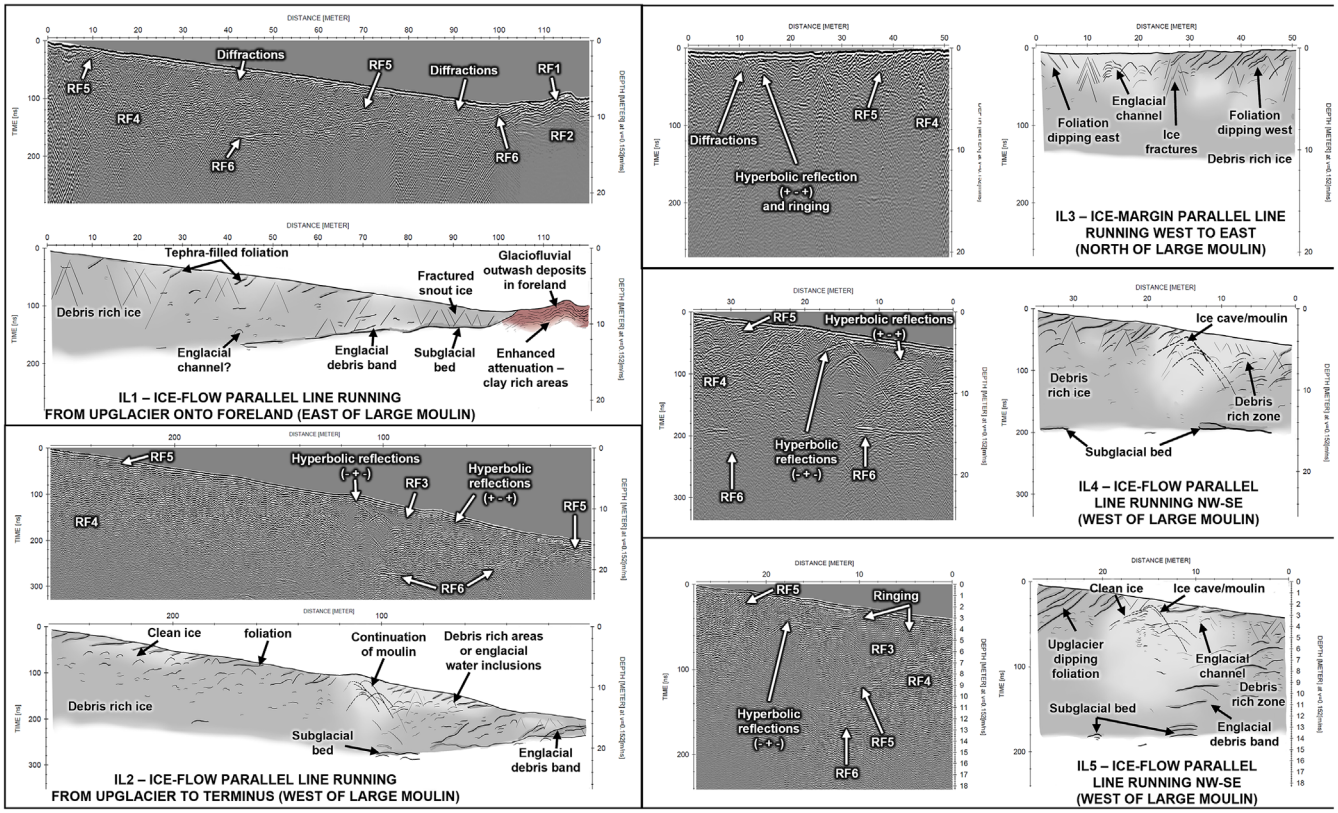

FIGURE 8 On-ice GPR profiles and their associated interpretation. The location of each profile is shown in Figure 1c. IL1 runs from upglacier down to the foreland sediments (160 MHz); IL2 runs upglacier down towards the active ice-margin, west of the large moulin (Figure 3b). IL3 runs west to east upglacier from the moulin (160 MHz). IL4 (160 MHz) and IL5 (450 MHz) run between IL1 and the moulin. [Color figure can be viewed at wileyonlinelibrary.com]

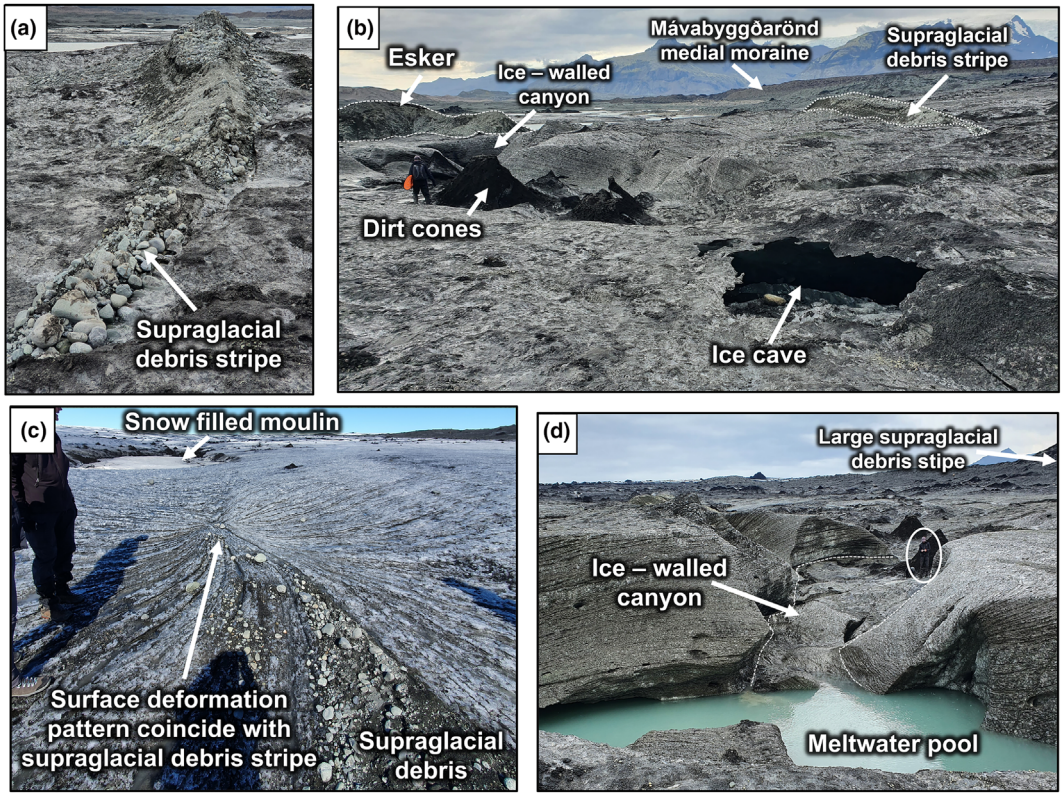

FIGURE 9 Selection of field photos: (a) supraglacial debris melting out of the ice (photo facing west); (b) the large moulin area in September 2022, the moulin has evolved into an ice-walled canyon; (c) deformation patterns on the surface of the ice. They appear to spread from a point which coincides with a supraglacial debris stripe. The May 2022 slow filled moulin is visible upglacier (photo facing north); (d) view upglacier of the previous moulin area which is now an ice-walled channel with meltwater pooling northeast of the September 2022 esker, circled person 1.8 m for scale (photo facing northeast). [Color figure can be viewed at wileyonlinelibrary.com]

Large reverse polarity (− + −) hyperbolae were imaged in the location directly southwest of the moulin (Figure 8, IL2). IL4 (160 MHz) and IL5 (450 MHz) were collected in the same area, and both contain the reverse polarity hyperbolae identified in IL2. The negative polarity indicates the waves are travelling through a material faster than the overlying glacial ice, therefore likely representing meltwater channels that are at least partially air-filled. The hyperbolae are deeper towards the downglacier end of the profile and are interpreted as the transition of the moulin into an englacial tunnel. By September 2022, the area where these lines were collected had evolved into a ~5-m-wide ice-walled and ice-floored canyon (Figure 9d), which supports the radargram interpretation. This tunnel, located upglacier of the esker, could have supplied sufficient supraglacial meltwater to the englacial environment to deposit the esker and the later meltwater channel running below the esker (Figure 7, EL5).

5 | DISCUSSION

5.1 | Englacial esker emergence: A conceptual model

A simplified six-stage conceptual model for the deposition and meltout of the ice-cored englacial esker is illustrated in Figure 10. This generalised model, which could apply to eskers of this type in general, does not account for the source of the sediment to the englacial conduit, which is likely to be dependent on local conditions (e.g. glacier structure, basal water pressures, bed geometry). After deposition of the glaciofluvial material in an enclosed glacial conduit (stage 1), the esker crest is exposed over time due to surface ablation and unroofing (stage 2). Stage 2 represents the broad-crested central area of the May 2022 esker. As the ice walls supporting the esker melt away, the sediments slump down each side (Stage 3). Although the central parts of the esker crest may be preserved (e.g. Figure 4j,k), the esker changes from broad-crested to round/sharp-crested. The slump deposits cover the surrounding ice at the base of the esker, resulting in an increase in the apparent footprint and amount of ice within the esker flanks, effectively transforming the esker into an ice-cored feature. Beyond the footprint of the esker, the surrounding ice melts at a faster rate due to less insulating debris cover.

Over time, this topographic inversion increases the esker prominence relative to the surrounding ice (stage 4). As downwasting and ice-margin retreat continues, the esker is lowered onto the foreland but still contains a significant ice core (stage 5). If there are no major changes to the drainage pattern, meltwater previously supplying the englacial channel can be redirected around the esker and may flow into or under the esker. If meltwater flows under the esker, it may speed up the melt of the ice core. Evidence of this was noted by the potential englacial channel imaged on GPR under the esker in the cross-profiles (e.g. Figure 7, EL5), and a tunnel was noted under the esker in September 2022 (Figure 4m). Channels running under or along the esker flanks have the potential to erode through the sediments and disrupt the continuity of the landform. Stage 5 is representative of most of the esker in September 2022.

As deglaciation progresses and the ice-core melts completely, under the right conditions, a ridge or ridge segments may be preserved. However, the esker may be unrecognisable in the deglaciated landscape due to continual sediment reworking as the ice melts away and by post-depositional processes such as erosion by meltwater (stage 6).

The evolution in esker morphology illustrated in Figure 10 was observed from the changes in crest shape and footprint over the 12-month observation period. Although local factors may have strong control on the deposition and post-depositional processes acting on englacial eskers, this model provides explanations for both the morphology and the geophysical signatures of the esker presented here and should be more widely applicable.

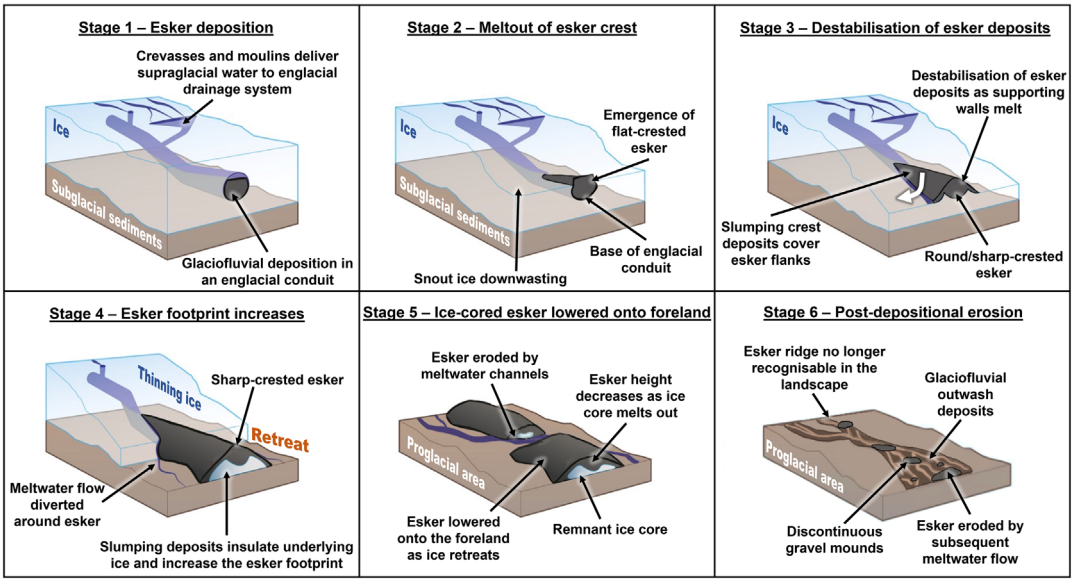

FIGURE 10 Simplified conceptual model for englacial esker evolution as they emerge from the ice. Six stages are presented from glaciofluvial deposition in an enclosed glacial conduit to the esker ridge being lowered onto the foreland as the ice-margin retreats. Note the change in esker morphology as the ridge is destabilised by the removal or supporting walls and meltout of buried ice. Once the ice retreats, the ice-cored esker may be subject to erosion by subsequent meltwater flow. [Color figure can be viewed at wileyonlinelibrary.com]

5.2 | Control on esker location: Meltwater and sediment sources

Supraglacial to subglacial meltwater routing is likely concentrated where flow units meet, as ice-flow patterns encourage longitudinal extension and transverse compression (Gulley, 2009; Price, 1969, 1973). Here, crevasses and lateral melt streams converge to provide a large meltwater supply (Gudmundsson & Bauder, 1999). At Breiðamerkurjökull, meltwater is concentrated along the medial moraine-ice contact (Storrar et al., 2015), which offers ample meltwater and sediment supply to create the large esker systems mapped in previous studies (e.g. Evans & Twigg, 2002; Price, 1969; Storrar et al., 2015). Although the esker is 900 m away from the nearest medial moraine (Mavabyggdarönd to the west), meltwater supply was clearly not an issue. Supraglacial meltwater streams converge on a trajectory towards the esker, in response to supraglacial topography, and can be become englacial via the large moulin and possibly smaller moulins located upglacier (north) of the esker (Figure 3).

Following Howarth (1968, 1971), it is likely that debris is delivered to the englacial environment through basal hydrofractures or shear planes and englacial debris was observed melting out of the glacier surface and potentially imaged in the radargrams (RF5). Rea & Evans (2011) demonstrated that the conditions required for surging are conducive to bottom-up hydrofracturing in surging glaciers and the central unit is known to have surged in the past. In addition, the normal polarity signature of RF5 represents a lower-velocity material than the surrounding glacial ice and resembles englacial debris bands found in GPR profiles by Burke et al. (2009) and Garabato et al. (2017).

An alternative source of sediment could be related to surging activity where foreland sediments are overridden during a surge and entrained into the ice margin, which then supplies sediment to englacial channels (Evans & Twigg, 2002). However, surges are rare and are less common in the central unit than the eastern one. The most recent recorded surge was in 1978 (Björnsson, 2003), and there is no indication of a surge having occurred in this section of the glacier in recent years, either from the geomorphology or the remote sensing record (Guðmundsson et al., 2017). Englacial eskers created by surging glaciers have a 'zig-zag' morphology (e.g. Evans et al., 2007; Evans & Rea, 2003; Kjær et al., 2008; Knudsen, 1995; Schomacker et al., 2014) unlike the landform presented in this work, further indicating the esker has not formed in response to a surge event.

The primary stratification and foliations in the ice are deformed upglacier of prominent debris stripes of the central unit (Figure 11). Folding of primary stratification is common in a zone of compressional flow (Jennings & Hambrey, 2021). The elevated water pressures (required to initiate basal hydrofracturing) and compressive ice flow in the study area are likely consequences of the glacier retreating across a retrograde bed (Figure 10, IL1 and IL2), like those examined by Spedding & Evans (2002), Bennett & Evans (2012) and Evans et al. (2023). Meltwater that reaches the subglacial bed upglacier of the study site may be forced up the adverse slope of the overdeepening (e.g. Larson et al., 2010; Roberts & Tweed, 2002), and this pressurised water could initiate the propagation of basal hydrofractures. Roberts et al. (2000) note that sudden increases in basal water pressures are enough to initiate hydrofracturing. A groundwater upwelling was observed to the west of the esker study site, and previously observed at Breiðamerkurjökull (Boulton et al., 2007a), providing evidence for subglacial water in excess of the ice overburden pressure.

In downwasting glaciers, englacial conduit location is controlled by outwash fan deposition at the margin, which increases the base level of the glaciohydraulic system (Bennett & Evans, 2012; Evans et al., 2023; Phillips et al., 2017; Spedding & Evans, 2002). Recent englacial esker and outwash head process-form study at neighbouring Fjallsjökull-Hrútárjökull by Evans et al. (2023) highlights the preferential development of englacial rather than subglacial tunnels in the advanced stages of snout downwasting, as meltwater bypasses the bed of the overdeepening in response to the changes in base level.

The observations presented here reiterate that the Shrevian model (Shreve, 1972) cannot account for the complexity of the drainage systems found within glaciers or larger ice masses (Greenwood et al., 2016; Gulley, 2009). Glacier structure and the presence of weakness in the ice are fundamental in developing englacial hydrological networks while providing a sediment source and a pathway that can be exploited by meltwater (Bennett et al., 2000; Roberts et al., 2000). Rapid evolution of the drainage system, including an increase in moulins, englacial conduits and crevassing, occurs as a response to deglaciation (Catania & Neumann, 2010; Nienow et al., 1998). This rapid evolution may be captured by an increase in the occurrence of englacial eskers at contemporary glacier margins. As ice thins at the margin, englacial channels are more likely to encounter debris-rich basal ice and associated debris-filled fractures. Entrained debris in these structures can then be reworked by the englacial meltwater. Furthermore, englacial eskers may become more common at downwasting snouts due to changes in the glacial hydrology associated with overdeepenings (Evans et al., 2023).

5.3 | Equifinality and preservation potential of englacial eskers

The form of an englacial esker crest is often taken as an indication of channel geometry and its position relative to the ice surface. Sharp-crested morphologies attained after the esker has emerged from the ice may indicate a deep narrow channel or a quasi-circular channel geometry (Price, 1973), the latter representing the englacial esker presented in this work. Sharp-crested Type 2 eskers described by Perkins et al. (2016) form in supraglacial or near surface englacial channels and are dominated by post-depositional faulting and vertical accretion, consistent with the esker crestline radargram. However, this study demonstrates that the esker shape can vary rapidly through time in response to post-depositional processes.

Englacial eskers are especially prone to sediment remobilisation during and following deposition due to meltout of the surrounding and underlying ice. Esker crest shape and planform are likely transient, controlled by post-depositional processes until they reach a stage where all ice has melted, and the sediments have reached their angle of repose. Using the crest shape of englacial eskers to infer the environment in which they were deposited should be done with caution.

This work demonstrates that englacial esker ridges evolve from flat to sharp-crested as they melt out and are reworked after deposition. In addition, segments of the esker eroded by meltwater, either

post-depositional by proglacial streams or syn-depositional by englacial channels, could be mistaken for periods of non-deposition (Perkins et al., 2016). Zig-zag eskers, also formed englacially by exploiting crevasse networks, have been observed to form at modern surging glaciers (e.g. Evans et al., 2007; Kjær et al., 2008; Ólafsdóttir, 2011; Schomacker et al., 2014) and may be represented by discontinuous gravel spreads and mounds in the palaeoglaciological record rather than being preserved as single ridges (Evans & Rea, 1999). Thus, they could look like the esker observed here, and distinguishing between the two types would be challenging without a detailed morphological/sedimentological study and determination of the associated landsystem, which is often hindered by the preservation potential of these landforms. This highlights the importance of accounting for esker equifinality when inferring drainage system characteristics from eskers (Storrar et al., 2020).

There are rare examples of eskers mapped in marine glaciated environments (Newton & Huuse, 2017; Ottesen et al., 2008; Todd et al., 2022; Todd & Shaw, 2012). In the case of englacial eskers formed at marine-terminating glaciers, they would likely have disturbed morphologies due to meltout of buried ice, or they may be transported away from the ice margin within calved icebergs (Ottesen et al., 2008). Therefore, like eskers deposited terrestrially, marine englacial eskers are unlikely to be preserved in single ridges.

The preservation potential for eskers such as the one presented here is potentially poor for two main reasons: gravitational collapse due to ice-core meltout and lateral erosion by meltwater. Even if mounds of esker deposits are preserved in the landscape once the ice core has melted out and erosion has ceased, much of the vital information will be lost, as the primary stratigraphy and structures are disrupted.

5.4 | Comparisons with other ice-cored eskers at Breiðamerkurjökull

No other englacial eskers were observed melting out of the ice margin during the field campaigns for this study, either from field observations or UAV surveys undertaken across the entire margin of the central flow unit. However, similar landforms were observed melting out of the ice-margin between 1951 and 1965. The evolution of these eskers, from available aerial imagery, is presented in Figure 11. Eskers 1 and 2 were examined by Price (1969) and Esker 3 by Howarth (1971).

Esker 1 was a 20-m high, sharp-crested sinuous ridge composed of stratified gravels (Price, 1969). In 1965, the proximal end of the ridge appeared to emerging from the Mávabyggðarönd medial moraine with the ridge extending out into the foreland. Field observations by Price (1969) found a meltwater channel flowing under and cross-cutting the esker, which caused part of the esker to collapse over the 1966 melt season. Trenched esker profiles revealed up to 5 m of glaciofluvial sediment overlying an ice core. From 1966 to 1967, Price (1969) noted esker lowering of up to 7 m in response to slumping and buried ice meltout. Esker 1 has not been preserved in the landscape, as the 2007 aerial imagery shows almost no trace of it apart from sparse gravel mounds.

Esker 2 had a similar morphology to Esker 1 but was only 5 m high. Aerial imagery for 1951 shows the esker melting out of the ice margin and sitting in a supraglacial position, similar to the May 2022 esker presented here. It was deposited less than 200 m from the Mávabyggðarönd medial moraine. From the 2007 imagery, Esker 2 has evolved into a spread of gravel mounds and segmented ridges.

Esker 3 was monitored melting out of the ice from 1965 to 1968 by (Howarth, 1968, 1971). The esker extended 50 m upglacier over a

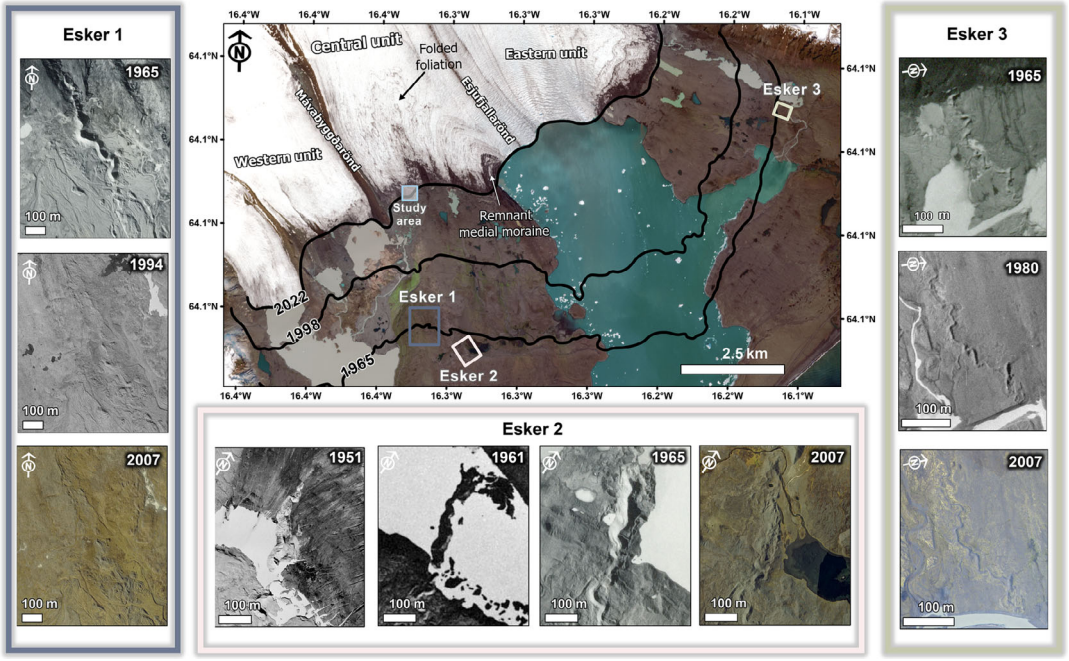

FIGURE 11 Aerial imagery time series for the eskers emerging from the ice margin of Breiðamerkurjökull and a map of their location in terms of the study area presented in this work (bright blue box). Esker 1 (dark blue extent) and esker 2 (pink extent) were examined by Price (1969) and are located along the axis of the Mavabyggdarönd medial moraine. Esker 3 (green extent) was examined by Howarth (1971) and emerged from the ice margin of the eastern unit (centre basemap Sentinel-2 harmonised true colour image 6 May 2022, aerial photographs were obtained from Landmælingar Islands and NERC ARSF). [Color figure can be viewed at wileyonlinelibrary.com]

1-year period, and the ridge was 15–20 m wide. On-ice portions of the esker were up to 5 m high. Similar to Esker 2, a meltwater stream cross-cut the esker and eroded through part of the landform between 1966 and 1968. By 2007, the portion of the esker that was observed to be englacial in origin (e.g. the proximal end in 1965) was not preserved as a prominent esker ridge but as a series of gravel mounds. However, the remaining portion of the esker was preserved as a single ridge. Although the emergence of this portion of the esker was not captured on the aerial imagery, it may also have an englacial origin, which further highlights that, under the right conditions, englacial eskers may be preserved in the landscape.

These examples from Breiðamerkurjökull provide further evidence that the esker presented in this paper may not be preserved in the landscape. However, the formation of these eskers suggests Breiðamerkurjökull may have a widespread, well-developed englacial drainage system, which has implications for the Boulton et al. (2007b) theory of groundwater and channel coupling.

5.5 | Implications for modelling glacial drainage systems and palaeo-ice sheet reconstructions

It has been theorised that the spacing of meltwater channels, which are recorded by eskers, is controlled by the balance between meltwater supply and permeability of subglacial substrate (Boulton et al., 2001; Boulton, 2007; Boulton et al., 2007b, 2009). Storrar et al. (2015) noted that the Boulton et al. (2007b) theory explained esker spacing at a large scale but found that local factors at Breiðamerkurjökull determined the meltwater and sediment supply, both of which exert important controls on esker deposition. Furthermore, the esker presented in this study, and those examined by Price (1969) and Howarth (1971), formed in an englacial position. Meltwater responsible for englacial esker deposition does not necessarily reach the ice-bed interface, and therefore, their formation is not controlled by groundwater conditions. Englacial eskers represent a component of the glacial drainage system that is not captured in the esker spacing theory of Boulton et al. (2007b). An assessment of the implications of this is beyond the scope of this paper, but an assessment of their spatial frequency could reasonably provide a first-order approximation of how important this could be. However, to fully assess, this would likely take multi-year UAV surveys and or a substantial GPR survey across the ice margin.

Meltwater pathways are complex and operate over various spatial and temporal scales. For reconstructing drainage systems in palaeo-environments, the landscape left behind should ideally be representative of the entire deglaciation. However, short-lived drainage events and their products, such as englacial eskers, may be lost, due to their poor preservation potential, thus limiting estimates of the amount of meltwater present during deglaciation by mapping preserved eskers alone.

5.6 | Research limitations and future research suggestions

The morphology and orientation of englacial channels can change over metre scales, which suggests that speleological surveys can only provide direct observations on the interior of the channel and not the dynamics or overall morphology due to their limited spatial resolution (Kamintzis et al., 2018). 3D GPR surveys across emerging eskers may allow examination of spatial variability in channel geometry over larger areas.

Although GPR is useful in providing subsurface information in a non-invasive, fast and cost-effective manner, its use is restricted by surface roughness and steep gradients. Crevasses, moulins and ice-collapse structures are common at the glacier margins, and their presence creates hazardous surveying conditions. Airborne GPR surveys would be a safer and more suitable approach in such environments (Church et al., 2021; Santin et al., 2019).

GPR interpretation also relies heavily on a solid understanding of the subsurface. As seen here, the complexity and wide range of potential sources of reflections makes interpretation challenging, particularly when the aim of the survey is to obtain accurate depths of subsurface features as the substrate velocity cannot be accurately estimated. Re-occupying survey lines and observations can aid in interpreting the profiles as the subsurface features are revealed by glacier thinning and retreat. As Breiðamerkurjökull is a soft-bedded glacier, the contrast between the unconsolidated subglacial sediments and debris-rich ice is minimal compared to a cold-based glacier frozen to bedrock. As active temperate glaciers are at, or near, pressure melting point throughout the year, the presence of liquid water and englacial water inclusions will increase signal attenuation and scattering, which will degrade the overall quality of the GPR data. GPR can still provide useful information but should be used in conjunction with additional data sources.

This work highlights the value of UAVs for geomorphological mapping and process-form studies, which has become a popular approach in recent years (Chandler et al., 2016, 2020; Ely et al., 2017; Evans et al., 2016, 2023; Hackney & Clayton, 2015; Tomczyk et al., 2019). UAV surveys have filled the spatial resolution mismatch between field geomorphology and aerial/satellite remote sensing data (Śledź et al., 2021). The esker described here is barely distinguishable in satellite imagery due to its size and the lack of contrast between the landform and the debris-covered ice margin. High-resolution DEMs also provide important information for quantifying changes over time that cannot be achieved by the use of satellite or aerial imagery alone.

Although the model presented in Figure 10 applies to the englacial esker examined in this work and potentially three ice-cored eskers at Breiðamerkurjökull examined by Price (1969) and Howarth (1971) (Figure 11), future work could test the applicability of the model to englacial eskers in other glacierised environments. In addition, with the increased use of high-resolution DEMs, there is more scope for mapping complex palaeo-landforms in detail (Delaney et al., 2018; Dewald et al., 2021). However, the identification of englacial eskers across palaeo-glaciated terrain will remain challenging.

6 | CONCLUSION

This study provides valuable insights into the morphological evolution and the internal architecture of an englacial esker as it emerged from the ice margin. The main findings contribute to englacial esker process-form relationships along with improving our understanding of their preservation potential while highlighting implications for palaeo-glacial drainage system reconstructions.

The esker core is composed of undulating beds of glaciofluvial sediments, usually deposited in a semi-circular basin, underlain by fine-grained sediments that attenuate the radar signal. Morphological analysis and internal architecture indicate the esker was deposited within a near-surface englacial conduit where the meltwater exploited structural weaknesses in the ice. Meltwater was supplied via a large moulin upglacier to the north, and the englacial continuation of the moulin was imaged on the radargrams as large reverse polarity hyperbolae. Over the 2022 meltwater season, this englacial tunnel evolved into an ice-walled canyon.

This work provides insights into the processes driving the formation of englacial eskers, with a potential link to an overdeepening at the study site. Meltwater delivered to the bed upglacier of the esker location becomes pressurised as it rises an adverse slope, resulting in basal hydrofracturing. These hydrofractures are infilled with sediment, providing a source of material that can be reworked by englacial meltwater. The englacial conduit formed by exploiting existing structures within the ice remains in an englacial position to bypass the overdeepening, a process that has been observed at other Icelandic glaciers.

The process-form model for englacial eskers emphasises their transient nature, as their crest morphology and planform change due to ridge destabilisation from buried ice meltout and erosion from subsequent meltwater flow. Although the impact of these post-depositional processes will vary depending on local conditions (e.g. proglacial meltwater pathways), the preservation potential of these eskers may be poor.

The presence of substantial englacial channels, identified by associated englacial eskers, has implications for using preserved esker spacing to estimate meltwater production during deglaciation. Such understanding is critical for validating hydrology parameterisations in numerical ice-flow models.

AUTHOR CONTRIBUTIONS

Project conceptualisation and methodological development by AL with support of AR, AWMN and BR. AL, AMWN and RDS secured funding. UAV data collection by TK, RDS and CG with UAV processing by TK. GPR data collected by AL, AR and MC. All GPR processing and GIS analysis was completed by AL. First draft written by AL with subsequent revisions from MS, BR, RDS, AR and AMWN. All software supplied by and licensed under Queen's University Belfast. All authors approved the submitted version of the manuscript.

ACKNOWLEDGEMENTS

AL was funded by UKRI QUADRAT Doctoral Training Programme (DTP) studentship (NE/S007377/1) and the Soulby Research Fund (QUB). AMWN would like to thank the British Society for Geomorphology Early Career Researcher fund. RDS received funding from the Quaternary Research Association. We wish to thank David Evans and one anonymous reviewer for their valuable input and detailed suggestions, which improved the final manuscript. We are especially grateful to Sigurður Óskar Jónsson of Vatnajökull National Park for supplying our research permits. We would also like to thank Haukur Ingi Einarsson of Glacier Adventure for helping with equipment postage and storage. Aerial photographs (1951-2007) were obtained from Landmælingar Islands and NERC ARSF.

CONFLICT OF INTEREST STATEMENT

All authors identify no conflict of interest.

DATA AVAILABILITY STATEMENT

Data are available upon request from the corresponding author.

ORCID

Amy Lally https://orcid.org/0000-0002-3406-0920

REFERENCES

Annan, P. (2009) Electromagnetic principles of ground penetrating radar. In: *Ground penetrating radar*. Amsterdam: Elsevier, pp. 1–40 https://doi.org/10.1016/B978-0-444-53348-7.00001-6

Aylsworth, J.M. & Shilts, W.W. (1989) Bedforms of the Keewatin ice sheet, Canada. *Sedimentary Geology*, 62(2–4), 407–428. Available from: https://doi.org/10.1016/0037-0738(89)90129-2

Benn, D., Gulley, J., Luckman, A., Adamek, A. & Glowacki, P.S. (2009) Englacial drainage systems formed by hydrologically driven crevasse propagation. *Journal of Glaciology*, 55(191), 513–523. Available from: https://doi.org/10.3189/002214309788816669

Benn, D.I. & Evans, D.J.A. (2010) *Glaciers and glaciation*, 2nd edition. London: Hodder Education.

Bennett, G.L. & Evans, D.J.A. (2012) Glacier retreat and landform production on an overdeepened glacier foreland: the debris-charged glacial landsystem at Kviárjökull, Iceland. *Earth Surface Processes and Landforms*, 37(15), 1584–1602. Available from: https://doi.org/10.1002/ESP.3259

Bennett, M.R., Huddart, D. & Waller, R.I. (2000) Glaciofluvial crevasse and conduit fills as indicators of supraglacial dewatering during a surge, Skeioararjokull, Iceland. *Journal of Glaciology*, 46(152), 25–34. Available from: https://doi.org/10.3189/172756500781833232

Beres, M. & Haeni, F.P. (1991) Application of ground-penetrating-radar methods in hydrogeologie studies. *Ground Water*, 29(3), 375–386. Available from: https://doi.org/10.1111/J.1745-6584.1991.TB00528.X

Björnsson, H. (2003) Subglacial lakes and jökulhlaups in Iceland. *Global and Planetary Change*, 35(3–4), 225–271. Available from: https://doi.org/10.1016/S0921-8181(02)00130-3

Boon, S. & Sharp, M.J. (2003) The role of hydrologically-driven ice fracture in drainage system evolution on an Arctic glacier. *Geophysical Research Letters*, 30(18), 1–3. Available from: https://doi.org/10.1029/2003GL018034

Boulton, G.S. (2007) Glaciers and their coupling with hydraulic and sedimentary processes. In: *Glacier science and environmental change*. Malden, MA: John Wiley and Sons, pp. 2–22 https://doi.org/10.1002/9780470750636.ch2

Boulton, G.S., Dobbie, K.E. & Zatsepin, S. (2001) Sediment deformation beneath glaciers and its coupling to the subglacial hydraulic system. *Quaternary International*, 86(1), 3–28. Available from: https://doi.org/10.1016/S1040-6182(01)00048-9

Boulton, G.S., Hagdorn, M., Maillot, P.B. & Zatsepin, S. (2009) Drainage beneath ice sheets: groundwater-channel coupling, and the origin of esker systems from former ice sheets. *Quaternary Science Reviews*, 28(7–8), 621–638. Available from: https://doi.org/10.1016/j.quascirev.2008.05.009

Boulton, G.S., Lunn, R., Vidstrand, P. & Zatsepin, S. (2007a) Subglacial drainage by groundwater-channel coupling, and the origin of esker systems: part 1-glaciological observations. *Quaternary Science Reviews*, 26(7–8), 1067–1090. Available from: https://doi.org/10.1016/j.quascirev.2007.01.007

Boulton, G.S., Lunn, R., Vidstrand, P. & Zatsepin, S. (2007b) Subglacial drainage by groundwater-channel coupling, and the origin of esker systems: part II-theory and simulation of a modern system. *Quaternary Science Reviews*, 26(7–8), 1091–1105. Available from: https://doi.org/10.1016/j.quascirev.2007.01.006

Brennand, T.A. (2000) Deglacial meltwater drainage and glaciodynamics: inferences from Laurentide eskers, Canada. *Geomorphology*, 32(3–4),

263–293. Available from: https://doi.org/10.1016/S0169-555X(99)00100-2

Burke, M.J., Woodward, J., Russell, A.J. & Fleisher, P.J. (2009) Structural controls on englacial esker sedimentation: Skeiðarárjökull, Iceland. *Annals of Glaciology*, 50(51), 85–92. Available from: https://doi.org/10.3189/172756409789097568

Burke, M.J., Woodward, J., Russell, A.J., Fleisher, P.J. & Bailey, P.K. (2008) Controls on the sedimentary architecture of a single event englacial esker: Skeiðarárjökull, Iceland. *Quaternary Science Reviews*, 27(19–20), 1829–1847. Available from: https://doi.org/10.1016/J.QUASCIREV.2008.06.012

Catania, G.A. & Neumann, T.A. (2010) Persistent englacial drainage features in the Greenland ice sheet. *Geophysical Research Letters*, 37(2), 1–5. Available from: https://doi.org/10.1029/2009GL041108

Catania, G.A., Neumann, T.A. & Price, S.F. (2008) Characterizing englacial drainage in the ablation zone of the Greenland ice sheet. *Journal of Glaciology*, 54(187), 567–578. Available from: https://doi.org/10.3189/002214308786570854

Chandler, B.M.P., Chandler, S.J.P., Evans, D.J.A., Ewertowski, M.W., Lovell, H., Roberts, D.H., et al. (2020) Sub-annual moraine formation at an active temperate Icelandic glacier. *Earth Surface Processes and Landforms*, 45(7), 1622–1643. Available from: https://doi.org/10.1002/esp.4835

Chandler, B.M.P., Evans, D.J.A. & Roberts, D.H. (2016) Characteristics of recessional moraines at a temperate glacier in SE Iceland: insights into patterns, rates and drivers of glacier retreat. *Quaternary Science Reviews*, 135, 171–205. Available from: https://doi.org/10.1016/J.QUASCIREV.2016.01.025

Church, G., Bauder, A., Grab, M. & Maurer, H. (2021) Ground-penetrating radar imaging reveals glacier's drainage network in 3D. *The Cryosphere*, 15(8), 3975–3988. Available from: https://doi.org/10.5194/tc-15-3975-2021

Church, G., Grab, M., Schmelzbach, C., Bauder, A. & Maurer, H. (2020) Monitoring the seasonal changes of an englacial conduit network using repeated ground-penetrating radar measurements. *The Cryosphere*, 14(10), 3269–3286. Available from: https://doi.org/10.5194/tc-14-3269-2020

Clark, P.U. & Walder, J.S. (1994) Subglacial drainage, eskers, and deforming beds beneath the Laurentide and Eurasian ice sheets. *Geological Society of America Bulletin*, 106(2), 304–314. Available from: https://doi.org/10.1130/0016-7606(1994)106<0304:SDEADB>2.3.CO;2

Cowton, T., Nienow, P., Sole, A., Wadham, J., Lis, G., Bartholomew, I., et al. (2013) Evolution of drainage system morphology at a land-terminating Greenlandic outlet glacier. *Journal of Geophysical Research: Earth Surface*, 118(1), 29–41. Available from: https://doi.org/10.1029/2012JF002540

Crameri, F. (2020) Scientific colour maps. Retrieved August 8, 2022, from https://www.fabiocrameri.ch/colourmaps/

Crameri, F., Shephard, G.E. & Heron, P.J. (2020) The misuse of colour in science communication. *Nature Communications*, 11, 5444. Available from: https://doi.org/10.1038/s41467-020-19160-7

Das, S.B., Joughin, I., Behn, M.D., Howat, I.M., King, M.A., Lizarralde, D., et al. (2008) Fracture propagation to the base of the Greenland ice sheet during supraglacial lake drainage. *Science*, 320(5877), 778–781. Available from: https://doi.org/10.1126/science.1153360

Delaney, C.A., McCarron, S. & Davis, S. (2018) Irish ice sheet dynamics during deglaciation of the central Irish midlands: evidence of ice streaming and surging from airborne LiDAR. *Geomorphology*, 306, 235–253. Available from: https://doi.org/10.1016/J.GEOMORPH.2018.01.011

Dewald, N., Lewington, E., Livingstone, S.J., Clark, C.D. & Storrar, R.D. (2021) Distribution, characteristics and formation of esker enlargements. *Geomorphology*, 392, 107919. Available from: https://doi.org/10.1016/j.geomorph.2021.107919

Ely, J.C., Graham, C., Barr, I.D., Rea, B.R., Spagnolo, M. & Evans, J. (2017) Using UAV acquired photography and structure from motion techniques for studying glacier landforms: application to the glacial flutes at Isfallsglaciären. *Earth Surface Processes and Landforms*, 42(6), 877–888. Available from: https://doi.org/10.1002/esp.4044

Evans, D.J.A. (2003) *Glacial landsystems*. London: Arnold.

Evans, D.J.A. (2009) Glacial geomorphology at Glasgow. *Scottish Geographical Journal*, 125(3–4), 285–320. Available from: https://doi.org/10.1080/14702540903364310

Evans, D.J.A. (2011) Glacial landsystems of Satujökull, Iceland: a modern analogue for glacial landsystem overprinting by mountain icecaps. *Geomorphology*, 129(3-4), 225–237. Available from: https://doi.org/10.1016/j.geomorph.2011.01.025

Evans, D.J.A., Atkinson, N. & Phillips, E. (2020) Glacial geomorphology of the neutral hills uplands, southeast Alberta, Canada: the process-form imprints of dynamic ice streams and surging ice lobes. *Geomorphology*, 350, 106910. Available from: https://doi.org/10.1016/j.geomorph.2019.106910

Evans, D.J.A., Ewertowski, M. & Orton, C. (2016) Fláajökull (north lobe), Iceland: active temperate piedmont lobe glacial landsystem. *Journal of Maps*, 12(5), 777–789. Available from: https://doi.org/10.1080/17445647.2015.1073185

Evans, D.J.A., Ewertowski, M., Roberts, D.H. & Tomczyk, A.M. (2022) The historical emergence of a geometric and sinuous ridge network at the Hørbyebreen polythermal glacier snout, Svalbard and its use in the interpretation of ancient glacial landforms. *Geomorphology*, 406, 108213. Available from: https://doi.org/10.1016/j.geomorph.2022.108213

Evans, D.J.A., Ewertowski, M.W., Tomczyk, A. & Chandler, B.M.P. (2023) Active temperate glacial landsystem evolution in association with outwash head/depositional overdeepenings. *Earth Surface Processes and Landforms*, 48(8), 1573–1598. Available from: https://doi.org/10.1002/ESP.5569

Evans, D.J.A. & Orton, C. (2015) Heinabergsjökull and Skalafellsjökull, Iceland: active temperate piedmont lobe and outwash head glacial landsystem. *Journal of Maps*, 11(3), 415–431. Available from: https://doi.org/10.1080/17445647.2014.919617

Evans, D.J.A. & Rea, B.R. (1999) Geomorphology and sedimentology of surging glaciers: a land-systems approach. *Annals of Glaciology*, 28, 75–82. Available from: https://doi.org/10.3189/172756499781821823

Evans, D.J.A. & Rea, B.R. (2003) Surging glacier landsystem. In: *Glacial Landsystems*. London: Arnold, pp. 259–288.

Evans, D.J.A. & Twigg, D.R. (2000) Breiðamerkurjökull 1998. 1:30,000 scale map. University of Glasgow and Loughborough University.

Evans, D.J.A. & Twigg, D.R. (2002) The active temperate glacial landsystem: a model based on Breiðamerkurjökull and Fjallsjökull, Iceland. *Quaternary Science Reviews*, 21(20–22), 2143–2177. Available from: https://doi.org/10.1016/S0277-3791(02)00019-7

Evans, D.J.A., Twigg, D.R., Rea, B.R. & Shand, M. (2007) Surficial geology and geomorphology of the Brúuarjökull surging glacier landsystem. *Journal of Maps*, 3(1), 349–367. Available from: https://doi.org/10.1080/jom.2007.9710850

Ewertowski, M.W., Evans, D.J.A., Roberts, D.H., Tomczyk, A.M., Ewertowski, W. & Pleksot, K. (2019) Quantification of historical landscape change on the foreland of a receding polythermal glacier, Hørbyebreen, Svalbard. *Geomorphology*, 325, 40–54. Available from: https://doi.org/10.1016/j.geomorph.2018.09.027

Fiore, J., Pugin, A., Beres, M., Fiore, J., Pugin, A. & Beres, M. (2002) Sedimentological and GPR studies of subglacial deposits in the joux valley (Vaud, Switzerland): backset accretion in an esker followed by an erosive jökulhlaup. *Géographie Physique et Quaternaire Sedimentological*, 56(1), 19–32. Available from: https://doi.org/10.7202/008602ar

Fountain, A.G., Jacobel, R.W., Schlichting, R. & Jansson, P. (2005) Fractures as the main pathways of water flow in temperate glaciers. *Nature*, 433(7026), 618–621. Available from: https://doi.org/10.1038/nature03296

Fountain, A.G. & Walder, J.S. (1998) Water flow through temperate glaciers. *Reviews of Geophysics*, 36(3), 299–328. Available from: https://doi.org/10.1029/97RG03579

Garabato, A.C.N., Forryan, A., Dutrieux, P., Brannigan, L., Biddle, L.C., Heywood, K.J., et al. (2017) Vigorous lateral export of the meltwater outflow from beneath an Antarctic ice shelf. *Nature*, 542(7640), 219–222. Available from: https://doi.org/10.1038/nature20825

Greenwood, S.L., Clason, C.C., Helanow, C. & Margold, M. (2016) Theoretical, contemporary observational and palaeo-perspectives on ice

sheet hydrology: processes and products. *Earth-Science Reviews*, 155, 1–27. Available from: https://doi.org/10.1016/j.earscirev.2016.01.010

Gudmundsson, G.H. & Bauder, A. (1999) Towards an indirect determination of the mass-balance distribution of glaciers using the kinematic boundary condition. *Geografiska Annaler Series A*, 81(4), 575–583. Available from: https://doi.org/10.1111/j.0435-3676.1999.00085.x

Guðmundsson, S., Björnsson, H. & Pálsson, F. (2017) Changes of Breiðamerkurjökull glacier, SE-Iceland, from its late nineteenth century maximum to the present. *Geografiska Annaler, Series A: Physical Geography*, 99(4), 338–352. Available from: https://doi.org/10.1080/04353676.2017.1355216

Guðmundsson, S., Björnsson, H., Pálsson, F., Magnússon, E., Sæmundsson, Þ. & Jóhannesson, T. (2019) Terminus lakes on the south side of Vatnajökull ice cap, SE-Iceland. *Jökull*, 69, 1–34. Available from: https://doi.org/10.33799/jokull2019.69.001

Guðmundsson, S. & Evans, D.J.A. (2022) Geomorphological map of Breiðamerkursandur 2018: the historical evolution of an active temperate glacier foreland. *Geografiska Annaler, Series A: Physical Geography*, 104(4), 298–332. Available from: https://doi.org/10.1080/04353676.2022.2148083

Gulley, J. & Benn, D.I. (2007) Structural control of englacial drainage systems in Himalayan debris-covered glaciers. *Journal of Glaciology*, 53(182), 399–412. Available from: https://doi.org/10.3189/002214307783258378

Gulley, J.D. (2009) Structural control of englacial conduits in the temperate Matanuska glacier, Alaska, USA. *Journal of Glaciology*, 55(192), 681–690. Available from: https://doi.org/10.3189/002214309789470860

Gulley, J.D., Benn, D.I., Screaton, E. & Martin, J. (2009) Mechanisms of englacial conduit formation and their implications for subglacial recharge. *Quaternary Science Reviews*, 28(19-20), 1984–1999. Available from: https://doi.org/10.1016/j.quascirev.2009.04.002

Gulley, J.D., Spellman, P.D., Covington, M.D., Martin, J.B., Benn, D.I. & Catania, G. (2014) Large values of hydraulic roughness in subglacial conduits during conduit enlargement: implications for modeling conduit evolution. *Earth Surface Processes and Landforms*, 39(3), 296–310. Available from: https://doi.org/10.1002/esp.3447

Gusmeroli, A., Murray, T., Barrett, B., Clark, R. & Booth, A. (2008) Estimates of water content in glacier ice using vertical radar profiles: a modified interpretation for the temperate glacier Falljökull, Iceland. *Journal of Glaciology*, 54(188), 939–942. Available from: https://doi.org/10.3189/002214308787779942

Hackney, C. & Clayton, A.I. (2015) Unmanned aerial vehicles (UAVs) and their application in geomorphic mapping. In: *Geomorphological techniques*. London, UK: British Society of Geomorphology.

Hansen, L.U., Piotrowski, J.A., Benn, D.I. & Sevestre, H. (2020) A cross-validated three-dimensional model of an englacial and subglacial drainage system in a high-Arctic glacier. *Journal of Glaciology*, 66(256), 278–290. Available from: https://doi.org/10.1017/jog.2020.1

Harrison, D., Ross, N., Russell, A.J. & Jones, S.J. (2022) *Ground-penetrating radar (GPR) investigations of a large-scale buried ice-marginal landsystem*, Skeiðarársandur, SE Iceland. Boreas. https://doi.org/10.1111/bor.12587

Howarth, P.J. (1968) Geomorphological and glaciological studies, eastern Breijamerkurjokull, Iceland. Unpublished Ph.D. Thesis. University of Glasgow.

Howarth, P.J. (1971) Investigations of two eskers at eastern Breiðamerkurjökull, Iceland. *Arctic and Alpine Research*, 3, 305–318.

Howarth, P.J. & Welch, R. (1969a) Breiðamerkurjökull, south-East Iceland, August 1945. 1:30,000 scale map. University of Glasgow.

Howarth, P.J. & Welch, R. (1969b) Breiðamerkurjökull, south-East Iceland, August 1965. 1:30,000 scale map. University of Glasgow.

Huddart, D., Bennett, M.R. & Glasser, N.F. (1999) Morphology and sedimentology of a high-arctic esker system: Vegbreen, Svalbard. *Boreas*, 28(2), 253–273. Available from: https://doi.org/10.1111/J.1502-3885.1999.TB00219.X

Jakobsen, P.R. & Overgaard, T. (2002) Georadar facies and glaciotectonic structures in ice marginal deposits, northwest Zealand, Denmark. *Quaternary Science Reviews*, 21(8–9), 917–927. Available from: https://doi.org/10.1016/S0277-3791(01)00045-2

Jennings, S.J.A. & Hambrey, M.J. (2021) Structures and deformation in glaciers and ice sheets. *Reviews of Geophysics*, 59(3), 1–135. Available from: https://doi.org/10.1029/2021RG000743

Joughin, I., Das, S.B., King, M.A., Smith, B.E., Howat, I.M. & Moon, T. (2008) Seasonal speedup along the western flank of the Greenland ice sheet. *Science*, 320(5877), 781–783. Available from: https://doi.org/10.1126/science.1153288

Kamintzis, J.E., Jones, J.P.P., Irvine-Fynn, T.D.L., Holt, T.O., Bunting, P., Jennings, S.J.A., et al. (2018) Assessing the applicability of terrestrial laser scanning for mapping englacial conduits. *Journal of Glaciology*, 64(243), 37–48. Available from: https://doi.org/10.1017/jog.2017.81

Karušs, J., Lamsters, K., Ješkins, J., Sobota, I. & Džeriņš, P. (2022) UAV and GPR data integration in glacier geometry reconstruction: a case study from Irenebreen, Svalbard. *Remote Sensing*, 14(3), 456. Available from: https://doi.org/10.3390/rs14030456

Kjær, K.H., Korsgaard, N.J. & Schomacker, A. (2008) Impact of multiple glacier surges - a geomorphological map from Brúarjökull, East Iceland. *Journal of Maps*, 4(1), 5–20. Available from: https://doi.org/10.4113/jom.2008.91

Knudsen, Ó. (1995) Concertina eskers, Brúarjökull, Iceland: an indicator of surge-type glacier behaviour. *Quaternary Science Reviews*, 14(5), 487–493. Available from: https://doi.org/10.1016/0277-3791(95)00018-K

Lamsters, K., Ješkins, J., Sobota, I., Karušs, J. & Džeriņš, P. (2022) Surface characteristics, elevation change, and velocity of high-Arctic valley glacier from repeated high-resolution UAV photogrammetry. *Remote Sensing*, 14(4), 1029. Available from: https://doi.org/10.3390/rs14041029

Larson, G.J., Lawson, D.E., Evenson, E.B., Knudsen, Ó., Alley, R.B. & Phanikumar, M.S. (2010) Origin of stratified basal ice in outlet glaciers of Vatnajökull and Öræfajökull, Iceland. *Boreas*, 39(3), 457–470. Available from: https://doi.org/10.1111/j.1502-3885.2009.00134.x

Lister, H. (1951) Report on glaciology at Breiðamerkurjökull 1951. *Jokull*, 3, 23–31.

Livingstone, S.J., Utting, D.J., Ruffell, A., Clark, C.D., Pawley, S., Atkinson, N., et al. (2017) Discovery of relict subglacial lakes and their geometry and mechanism of drainage. *Nature Communications*, 7(1), 1–9. Available from: https://doi.org/10.1038/ncomms11767

Lovell, H., Livingstone, S.J., Boston, C.M., Booth, A.D., Storrar, R.D. & Barr, I.D. (2019) Complex kame belt morphology, stratigraphy and architecture. *Earth Surface Processes and Landforms*, 44(13), 2685–2702. Available from: https://doi.org/10.1002/ESP.4696

Matsouka, K., Thorsteinsson, T., Björnsson, H. & Waddington, E.D. (2007) Anisotropic radio-wave scattering from englacial water regimes, Mýrdalsjökull, Iceland. *Journal of Glaciology*, 53(182), 473–478. Available from: https://doi.org/10.3189/002214307783258422

McDonald, B.C. & Shilts, W.W. (1975) Interpretation of faults in glaciofluvial sediments. In: *Glaciofluvial and glaciolacustrine sedimentation*. Tulsa: SEPM Society for Sedimentary Geology, pp. 123–131 https://doi.org/10.2110/pec.75.23.0123

Murray, T., Corr, H., Forieri, A. & Smith, A.M. (2008) Contrasts in hydrology between regions of basal deformation and sliding beneath Rutford ice stream, West Antarctica, mapped using radar and seismic data. *Geophysical Research Letters*, 35(12), 1–5, n/a. Available from: https://doi.org/10.1029/2008GL033681

Murray, T., Stuart, G.W., Fry, M., Gamble, N.H. & Crabtree, M.D. (2000) Englacial water distribution in a temperate glacier from surface and borehole radar velocity analysis. *Journal of Glaciology*, 46(154), 389–398. Available from: https://doi.org/10.3189/172756500781833188

Neal, A. (2004) Ground-penetrating radar and its use in sedimentology: principles, problems and progress. *Earth Science Reviews*, 66(3–4), 261–330. Available from: https://doi.org/10.1016/J.EARSCIREV.2004.01.004

Newton, A.M.W. & Huuse, M. (2017) Glacial geomorphology of the central Barents Sea: implications for the dynamic deglaciation of the Barents sea ice sheet. *Marine Geology*, 387, 114–131. Available from: https://doi.org/10.1016/J.MARGEO.2017.04.001

Nienow, P., Sharp, M. & Willis, I. (1998) Seasonal changes in the morphology of the subglacial drainage system, haut glacier d'Arolla, Switzerland. *Earth Surface Processes and Landforms*, 23, 825–843. Available from: https://doi.org/10.1002/(SICI)1096-9837(199809)23:9<825::AID-ESP893>3.0.CO;2-2

Ólafsdóttir, E. (2011) Myndun og þróun krákustígsása við Eyjabakkajökul.

Ottesen, D., Dowdeswell, J.A., Benn, D.I., Kristensen, L., Christiansen, H.H., Christensen, O., et al. (2008) Submarine landforms characteristic of glacier surges in two Spitsbergen fjords. *Quaternary Science Reviews*, 27(15–16), 1583–1599. Available from: https://doi.org/10.1016/j.quascirev.2008.05.007

Pellicer, X.M. & Gibson, P. (2011) Electrical resistivity and ground penetrating radar for the characterisation of the internal architecture of quaternary sediments in the midlands of Ireland. *Journal of Applied Geophysics*, 75(4), 638–647. Available from: https://doi.org/10.1016/J.JAPPGEO.2011.09.019

Perkins, A.J., Brennand, T.A. & Burke, M.J. (2013) Genesis of an esker-like ridge over the southern Fraser plateau, British Columbia: implications for paleo-ice sheet reconstruction based on geomorphic inversion. *Geomorphology*, 190, 27–39. Available from: https://doi.org/10.1016/J.GEOMORPH.2013.02.005

Perkins, A.J., Brennand, T.A. & Burke, M.J. (2016) Towards a morphogenetic classification of eskers: implications for modelling ice sheet hydrology. *Quaternary Science Reviews*, 134, 19–38. Available from: https://doi.org/10.1016/J.QUASCIREV.2015.12.015

Phillips, E., Everest, J., Evans, D.J.A., Finlayson, A., Ewertowski, M., Guild, A., et al. (2017) Concentrated, 'pulsed' axial glacier flow: structural glaciological evidence from Kviárjökull in SE Iceland. *Earth Surface Processes and Landforms*, 42(13), 1901–1922. Available from: https://doi.org/10.1002/esp.4145

Phillips, E., Finlayson, A. & Jones, L. (2013) Fracturing, block faulting, and moulin development associated with progressive collapse and retreat of a maritime glacier: Falljökull, SE Iceland. *Journal of Geophysical Research: Earth Surface*, 118(3), 1545–1561. Available from: https://doi.org/10.1002/jgrf.20116

Price, R.J. (1969) Moraines, Sandar, Kames and Eskers near Breiðamerkurjökull, Iceland. *Transactions of the Institute of British Geographers*, 46(46), 17–43. Retrieved from https://www.jstor.org/stable/621406. Available from: https://doi.org/10.2307/621406

Price, R.J. (1973) *Glacial and fluvioglacial landforms*. London: Longman.

Price, R.J. (1982) Changes in the proglacial area of Breiðamerkurjökull, southeastern Iceland: 1890–1980. *Jökull*, 32(1), 29–35. Available from: https://doi.org/10.33799/jokull1982.32.029

Price, R.J. & Howarth, P.J. (1970) The evolution of the drainage system (1904–1965) in front of Breiðamerkurjökull, Iceland. *Jökull*, 20(1), 27–37. Available from: https://doi.org/10.33799/jokull1970.20.027

Rea, B.R. & Evans, D.J.A. (2011) An assessment of surge-induced crevassing and the formation of crevasse squeeze ridges. *Journal of Geophysical Research: Earth Surface*, 116(4), F04005. Available from: https://doi.org/10.1029/2011JF001970

Roberts, M.J., Russell, A.J., Tweed, F.S. & Knudsen, Ó. (2000) Rapid sediment entrainment and englacial deposition during jökulhlaups. *Journal of Glaciology*, 46(153), 349–351. Available from: https://doi.org/10.3189/172756500781832936

Roberts, M.J. & Tweed, F.S. (2002) Glaciohydraulic supercooling in Iceland near the snouts of Piedmont glacier. *Geology*, 5, 439–442.

Rothlisberger, H. & Lang, H. (1987) Glacial hydrology. In: *Glaciofluvial sediment transfer*. New York: Wiley, pp. 207–284.

Sandmeier, K.J. (2006) ReflexW version 7.5.9. Karlsruhe, Germany.

Santin, I., Colucci, R.R., Žebre, M., Pavan, M., Cagnati, A. & Forte, E. (2019) Recent evolution of Marmolada glacier (Dolomites, Italy) by means of ground and airborne GPR surveys. *Remote Sensing of Environment*, 235, 111442. Available from: https://doi.org/10.1016/J.RSE.2019.111442

Schomacker, A., Benediktsson, Í.Ö. & Ingólfsson, Ó. (2014) The Eyjabakkajökull glacial landsystem, Iceland: geomorphic impact of multiple surges. *Geomorphology*, 218, 98–107. Available from: https://doi.org/10.1016/J.GEOMORPH.2013.07.005

Shreve, R.L. (1972) Movement of water in glaciers. *Journal of Glaciology*, 11(62), 205–214. Available from: https://doi.org/10.3189/s0022143000022219x

Shreve, R.L. (1985) Esker characteristics in terms of glacier physics, Katahdin esker system, Maine. *Geological Society of America Bulletin*, 96(5), 639–646. Available from: https://doi.org/10.1130/0016-7606(1985)96<639:ECITOG>2.0.CO;2

Śledź, S., Ewertowski, M. & Piekarczyk, J. (2021) Applications of unmanned aerial vehicle (UAV) surveys and structure from motion photogrammetry in glacial and periglacial geomorphology. *Geomorphology*, 378, 107620. Available from: https://doi.org/10.1016/j.geomorph.2021.107620

Spagnolo, M., King, E.C., Ashmore, D.W., Rea, B.R., Ely, J.C. & Clark, C.D. (2014) Looking through drumlins: testing the application of ground-penetrating radar. *Journal of Glaciology*, 60(224), 1126–1134. Available from: https://doi.org/10.3189/2014JoG14J110

Spedding, N. & Evans, D.J.A. (2002) Sediments and landforms at Kviárjökull, southeast Iceland: a reappraisal of the glaciated valley landsystem. *Sedimentary Geology*, 149(1-3), 21–42. Available from: https://doi.org/10.1016/S0037-0738(01)00242-1

Stenborg, T. (1969) Studies of the internal drainage of glaciers. *Geografiska Annaler, Series A: Physical Geography*, 51(A), 13–41. Available from: https://doi.org/10.1080/04353676.1969.11879788

Stoker, B.J., Livingstone, S.J., Barr, I.D., Ruffell, A., Storrar, R.D. & Roberson, S. (2021) Variations in esker morphology and internal architecture record time-transgressive deposition during ice margin retreat in Northern Ireland. *Proceedings of the Geologists' Association*, 132(4), 409–425. Available from: https://doi.org/10.1016/j.pgeola.2021.03.002

Storrar, R.D., Evans, D.J.A., Stokes, C.R. & Ewertowski, M. (2015) Controls on the location, morphology and evolution of complex esker systems at decadal timescales, Breiðamerkurjökull, southeast Iceland. *Earth Surface Processes and Landforms*, 40(11), 1421–1438. Available from: https://doi.org/10.1002/esp.3725

Storrar, R.D., Ewertowski, M., Tomczyk, A.M., Barr, I.D., Livingstone, S.J., Ruffell, A., et al. (2020) Equifinality and preservation potential of complex eskers. *Boreas*, 49(1), 211–231. Available from: https://doi.org/10.1111/bor.12414

Storrar, R.D., Stokes, C.R. & Evans, D.J.A. (2014) Morphometry and pattern of a large sample (>20,000) of Canadian eskers and implications for subglacial drainage beneath ice sheets. *Quaternary Science Reviews*, 105, 1–25. Available from: https://doi.org/10.1016/J.QUASCIREV.2014.09.013

Sutherland, J.L., Carrivick, J.L., Evans, D.J.A., Shulmeister, J. & Quincey, D.J. (2019) The Tekapo glacier, New Zealand, during the last glacial maximum: an active temperate glacier influenced by intermittent surge activity. *Geomorphology*, 343, 183–210. Available from: https://doi.org/10.1016/j.geomorph.2019.07.008

Temminghoff, M., Benn, D.I., Gulley, J.D. & Sevestre, H. (2019) Characterization of the englacial and subglacial drainage system in a high Arctic cold glacier by speleological mapping and ground-penetrating radar characterization of the englacial and subglacial drainag. *Geografiska Annaler: Series A, Physical Geography*, 101(2), 98–117. Available from: https://doi.org/10.1080/04353676.2018.1545120

Todd, B.J., Dowdeswell, J.A., Shaw, J., Campbell, D.C. & Mate, D.J. (2022) Deglacial dynamics of the Foxe–Baffin ice sheet, Frobisher Bay, Nunavut, Canada revealed by submarine landform mapping. *Journal of Quaternary Science*, 38, 365–385. Available from: https://doi.org/10.1002/jqs.3486

Todd, B.J. & Shaw, J. (2012) Laurentide ice sheet dynamics in the bay of Fundy, Canada, revealed through multibeam sonar mapping of glacial landsystems. *Quaternary Science Reviews*, 58, 83–103. Available from: https://doi.org/10.1016/j.quascirev.2012.10.016

Todtmann, E.M. (1960) Gletscherforschungen auf Island (Vatnajökull). Abhandlung aus dem Gebiet der Auslandskunde. Hamburg.

Tomczyk, A.M., Ewertowski, M.W., Stawska, M. & Rachlewicz, G. (2019) Detailed alluvial fan geomorphology in a high-arctic periglacial environment, Svalbard: application of unmanned aerial vehicle (UAV) surveys. *Journal of Maps*, 15(2), 460–473. Available from: https://doi.org/10.1080/17445647.2019.1611498

Van Overmeeren, R.A. (1998) Radar facies of unconsolidated sediments in the Netherlands: a radar stratigraphy interpretation method for hydrogeology. *Journal of Applied Geophysics*, 40(1–3), 1–18. Available from: https://doi.org/10.1016/S0926-9851(97)00033-5

Welch, R. & Howarth, P.J. (1968) Photogrammetric measurements of glacial landforms. *Photogrammetric Record*, 6(31), 75–96. Available from: https://doi.org/10.1111/j.1477-9730.1968.tb00915.x

Westoby, M.J., Brasington, J., Glasser, N.F., Hambrey, M.J. & Reynolds, J.M. (2012) "Structure-from-motion" photogrammetry: a low-cost, effective tool for geoscience applications. *Geomorphology*, 179, 300–314. Available from: https://doi.org/10.1016/j.geomorph.2012.08.021

Zwally, H.J., Abdalati, W., Herring, T., Larson, K., Saba, J. & Steffen, K. (2002) Surface melt-induced acceleration of Greenland ice-sheet flow. *Science*, 297(5579), 218–222. Available from: https://doi.org/10.1126/science.1072708

How to cite this article: Lally, A., Ruffell, A., Newton, A.M.W., Rea, B.R., Kahlert, T., Storrar, R.D. et al. (2023) The evolution and preservation potential of englacial eskers: An example from Breiðamerkurjökull, SE Iceland. *Earth Surface Processes and Landforms*, 48(14), 2864–2883. Available from: https://doi.org/10.1002/esp.5664